UNIVERSITY OF CALIFORNIA
Santa Barbara

Optimization of Microdroplet-based Techniques to Measure Mechanical Stresses in 3D Multicellular Systems

A Dissertation submitted in partial satisfaction
of the requirements for the degree of

Doctor of Philosophy

in

Mechanical Engineering

by

Adam Alan Michael Lucio
Committee in Charge:

Professor Otger Campàs, Chair

Dr. Adele Doyle, Principle Investigator/Lecturer

Professor Megan Valentine

Professor Robert McMeeking

Professor Todd Squires

January 2018

The Dissertation of
Adam Alan Michael Lucio is approved:

Dr. Adele Doyle, Principle Investigator/Lecturer

Professor Megan Valentine

Professor Robert McMeeking

Professor Todd Squires

Professor Otger Campàs, Committee Chairperson

December 2017

Optimization of Microdroplet-based Techniques to Measure Mechanical Stresses in 3D Multicellular Systems

by

Adam Alan Michael Lucio

To my parents who have always encouraged me to be the best that I can be.

To my brother, who has been an unparalleled role model throughout my life.

To my friends and family who have always supported me.

This is dedicated to you.

Acknowledgements

First and foremost, I would like to thank my advisor, Professor Otger Campàs, for guiding me through this challenging and rewarding experience during my Ph.D. Your mentorship and guidance was invaluable during this time, and has helped me grow as an individual and as a researcher. It has been a pleasure to work in the Campàs Lab, with so many wonderul people on such exciting research projects.

I would also like to thank my Ph.D. committee members. Thank you Dr. Adele Doyle for your close mentorship and guidance during my Ph.D. I thank Professor Megan Valentine, Professor Robert McMeeking, and Professor Todd Squires for their support, as well as their helpful comments and questions. You have all helped to guide me during my Ph.D. and your feedback has helped shape my research during graduate school.

I would like to acknowledge Dr. Tzu-Chi Kuo, whose guidance and direction during my undergraduate work at Dow Chemical led me to pursue my Ph.D. Thank you for being both a mentor and a friend. I am truly grateful to have had the privilege of working for you.

I would like to thank Professor Sumita Pennathur for her encouragement and support. My time spent working in the Nanolab during my undergraduate internship and initial work as a graduate student was a pleasure. Thank you for always being supportive, and for helping to create wonderful, life-changing opportunities for me.

I would like to thank Professor Frederic Gibou, who, during his time as department Chair and Advisor greatly helped to guide my Ph.D. Thank you for always making time to meet and discuss progress, plans and future steps.

Thank you to all members of the Campas Lab whom I have worked with over the past five years: thank you Alessandro, Friedhelm, Payam, Georgina, Elijah, Jamie, Mishel, David, James, Samhita, Carlos, Hannah, and Renwei. Working with such an amazing group of people has been an absolute pleasure. Thank you also to Carolin, and Athina of the Hawker Lab for your help during our collaborative work, and for your support outside of the laboratory. You have both helped me greatly during my Ph.D., and I could not have wished for a better collaboration.

I would like to also thank my undergraduate research assistants Asha and Gatuam. You have both been so helpful during my Ph.D., and I am so proud to see you both achieving your goals. It has been an honor to work with you, and a pleasure to mentor such wonderful, hard-working students.

Lastly, thank you to my family and friends, who have always been there for me. With unconditional encouragement and support, you have truly helped me through this experience.

CURRICULUM VITAE

Adam Alan Michael Lucio

EDUCATION

PhD in Mechanical Engineering, UC Santa Barbara **2012-Present**

BS in Mechanical Engineering, Saginaw Valley State University **2007-2012**

WORK EXPERIENCE

- **Graduate Student Researcher** **09/2012-Present**

  Mechanical Engineering Dept., University of California, Santa Barbara

- **R&D Laboratory Technician** **09/2007-08/2012**

  High Throughput R&D, The Dow Chemical Company, Midland, MI

- **Research Internship in Science and Engineering** **06/2011-08/2011**

  Mechanical Engineering Dept., University of California, Santa Barbara

PUBLICATIONS

- **Lucio, A. A.**, Ingber, D.E., and Campas, O. Generation of biocompatible droplets for *in vivo* and *in vitro* measurement of cell-generated mechanical stresses, *Biophysical Methods in Cell Biology* **2015**, 1, 373-390.

- **Lucio, A. A.**, Mongera, A., Shelton, E., Chen, R., Doyle, A.M., and Campas, O. Spatiotemporal variation of endogenous cell-generated stresses within 3D multicellular spheroids, *Scientific Reports* **2017**, 7(1), 12022.

– Serwane, F., Mongera, A., Rowghanian, P., Kealhofer, D.A., **Lucio, A. A.**, Hockenbery, Z.M., Campas, O. *In vivo* quantification of spatially varying mechanical properties in developing tissues, *Nature Methods* **2016**, 14(2), 181-186.

– Davies, E., Bishop, L., **Lucio, A.A.**, Del Bonis-O'Donnell, J.T., Pennathur, S., Fintschenko, Y. Field Amplified Sample Stacking (FASS) for Sample Concentration in a Nanochannel. **2012**. (LabSmith Application Note).

AWARDS

– Crossroads Fellowship in Materials, Mechanics and Medicine, UCSB **2015**

– Mellichamp Fellowship in Systems Biology, UCSB **2014**

– Mechanical Engineering Summer Fellowship, UCSB **2013, 2014**

– Honorable mention, Braun Award for Writing Excellence **2009**

CONFERENCE CONTRIBUTIONS

– **Lucio, A.A.** et al. Measuring stresses in living materials, *Mellichamp Cluster in Systems Biology and Bioengineering* (2017).

– **Lucio, A.A.** et al. Stress variations measured within multicellular spheroids, *UC Systemwide Bioengineering Symposium* (2016).

– **Lucio, A.A.** et al. Stress profiles in cellular spheroids: getting inside model tissues, *Mellichamp Cluster in Systems Biology and Bioengineering* (2016).

MENTORING EXPERIENCE

– Teaching Assistant, UC Santa Barbara **2012-2015**

– Undergraduate Research Mentor, UC Santa Barbara **2016-2017**

RELEVANT SKILLS

Microfluidics, optical tensiometry, confocal microscopy, ImageJ, Matlab, LaTeX

Abstract

Optimization of Microdroplet-based Techniques to Measure Mechanical Stresses in 3D Multicellular Systems

Adam Alan Michael Lucio

In addition to the well-established influence that soluble factors have on cellular behavior, physical forces are also now known to play a large role. Many cellular processes such as proliferation, apoptosis, differentiation, and mobility, have all been shown to be influenced by mechanical inputs. This has been demonstrated in developing embryos, and also during cancer progression, from tumor growth and invasion, to metastasis. Tools which enable the measurement of mechanical forces in a variety of systems *in vitro* and *in vivo* can enable a deeper understanding of the mechanical inputs that cells are receiving in 3D tissues, and enable quantification of stress patterns in these systems. My work encompasses the generation of droplets with well-controlled properties, used as force transducers to measure stresses within 3D, multicellular systems. By characterizing the interfacial tension, and by imaging the shape of droplets in 3D, anisotropic stresses can be measured. Precise control of the interfacial tension, droplet size, and cell-droplet interaction enables their use to accurately measure anisotropic stresses applied both *in vivo* and *in vitro*. Using these

droplets, I quantify spatiotemporal stresses within growing mesenchymal cell aggregates, in 3D.

First I describe a new surfactant system which allows for precise control over the interfacial tension of fluorocarbon oil droplets, while still mediating the interactions between droplets and surrounding cells. This surfactant system is resistant to changes in interfacial tension in complex chemical environments, with varying ionic strength and small molecules competing for the surface. These droplets are generated with devices and materials that are commercially available, making the technique openly accessible to most laboratories. Studies aimed at measuring mechanical stresses in a variety of systems either *in vivo* or *in vitro*, at different length scales (by controlling the droplet size), may make use of this method.

I then use these droplets to measure endogenous, anisotropic stresses within model tissues - 3D cellular spheroids. These experiments enable a spatiotemporal map of stresses to be generated from growing, 3D spheroids of mesenchymal cells. Stresses are quantified for both mediated adhesion, and hindered adhesion, between droplets and cells. This allowed the investigation of stress contributions from both tensile and compressive stresses (in the first case), and those solely due to compressive stresses (in the second case).

Lastly, I further enhance fluorocarbon oil-in-water emulsions in a collaborative project which includes the synthesis and characterization of new fluorosurfactants.

In contrast to previously established methods, these fluorosurfactants are generated from completely non-ionic starting materials, enabling their use in biological applications which may contain molecules (e.g proteins) susceptible to be influenced by charged surfactants. The new fluorosurfactants offer excellent long-term stabilization of fluorocarbon oil-in-water emulsions, without the need for additional co-surfactants.

Contents

List of Figures

List of Tables

Chapter 1

The Role of Mechanical Forces in Living Tissues

1.1 Introduction: Forces in Biological Systems

Viewing biological development through the scope of a mechanical approach was heavily inspired after the publication of D'Arcy Thompson's book *On Growth and Form* [1] in the early 1900's. That the growth and form of living organisms were dependent on physical forces was a revolutionary turn of the tide for understanding biological processes. Numerous examples began to emerge demonstrating that developmental processes and morphogenetic movements could be explained using physical concepts.

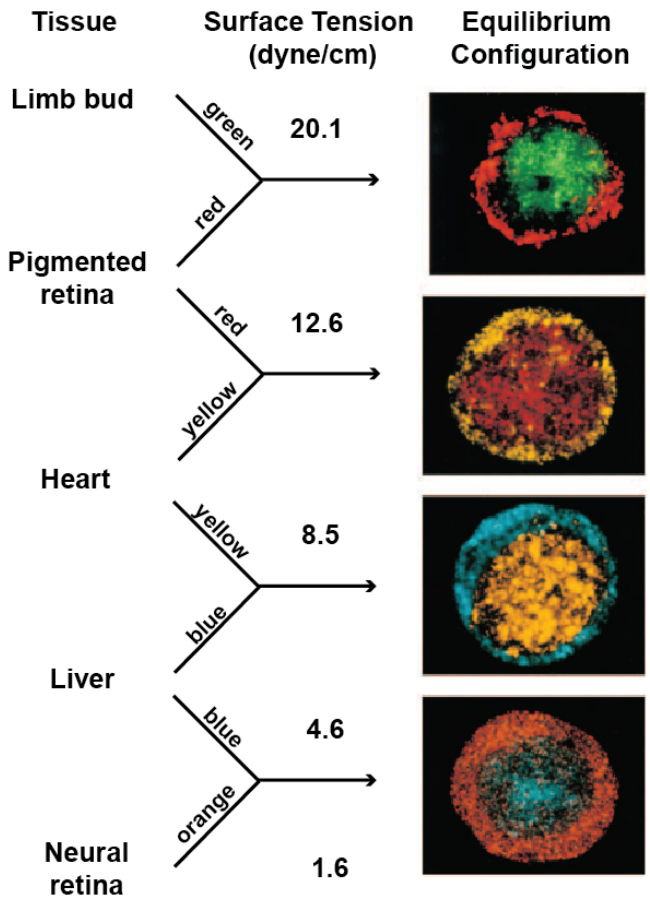

Figure 1.1: Surface tension regulates cell sorting of embryonic tissues. Five embryonic tissues, each labeled with contrasting fluorescent markers. Tissues characterized by a higher surface tension are always enveloped by tissues with a lower surface tension. Modified from [4].

In the 1960's, Steinberg hypothesized that two different tissues adjust their surface contact based on the principle of lowering the total interfacial free energy [2,3], much like two immiscible liquids with different surface energies. This would become known as the differential adhesion hypothesis (DAH). By quantifying the surface tension (arising from cohesive forces between cells) of cell aggregates derived from different embryonic germ layers, Steinberg and colleagues showed that cell aggregates characterized by larger intercellular adhesive forces (e.g. a higher surface tension) were

always enveloped by cell aggregates characterized with smaller intercellular adhesive forces (a lower surface tension) (Figure 1.1) [4].

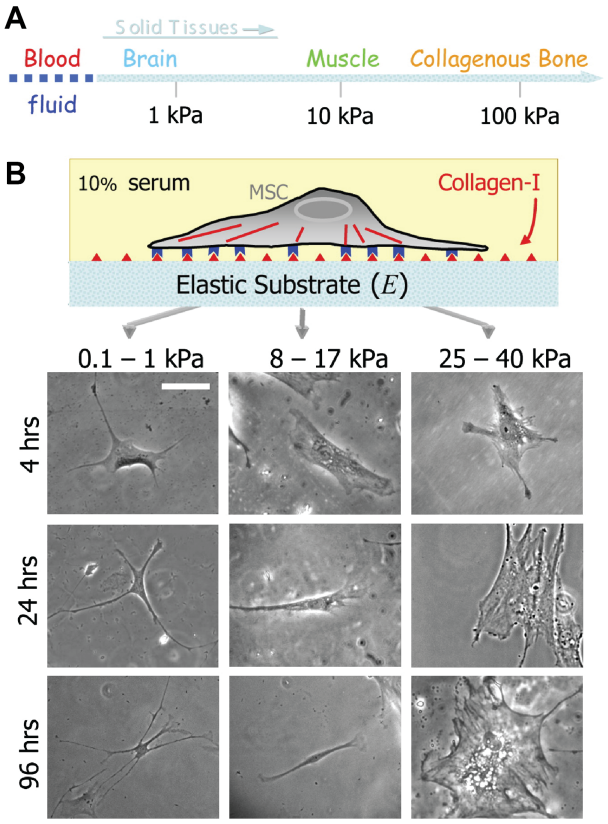

Figure 1.2: Mechanical influence on cell differentiation. (A) Solid tissues are characterized by different stiffness, or modulus of elasticity *E*. (B) Mesenchymal stem cells are plated to substrates of varying *E*, influencing their differentiation. Tuning the substrate stiffness to mimic that of brain, muscle and collagenous bone tissue induced differentiation into neurons, myoblasts and osteoblasts, respectively. Modified from [5].

In 2006, pioneering work by Engler *et al.* demonstrated that the fate of stem cells could be determined by tuning the mechanics of the microenvironment [5]. The stiffness (elasticity) of the microenvironment was tuned to mimic that of embryonic brain, muscle and collagenous bone tissue which induced MSC differentiation into neurons, myoblasts and osteoblasts, respectively (Figure 1.2). In line with these seminal studies, researchers spanning several scientific fields have investigated how physical forces and mechanics play a role in shaping biological systems, and studies have been per-

formed to observe how cellular behavior is affected by these mechanical cues. Such research has investigated the role that mechanical forces play in guiding cellular behaviors pertinent to development and growth of tissues, including cell proliferation (Figure 1.3, left) and apoptosis [6, 7, 8, 9, 10], cell adhesion [11, 12], cell differentiation [5, 13], and cell migration [14, 15, 16].

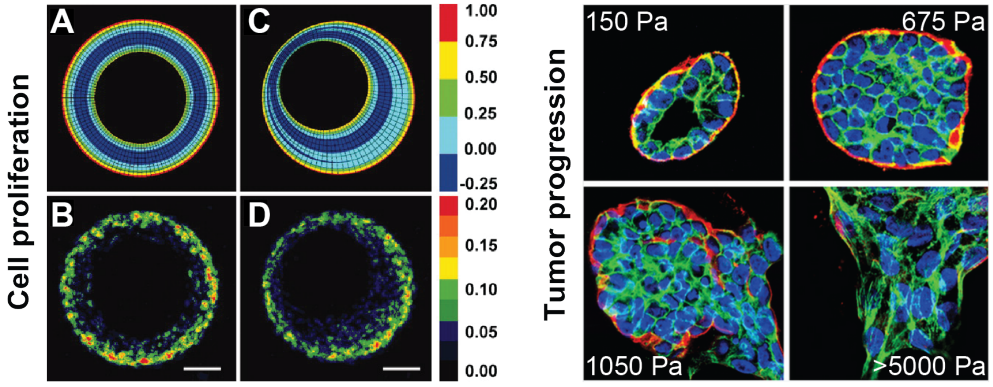

Figure 1.3: Mechanical influences in cellular behavior and disease progression. (Left) Patterns of cell proliferation correspond to distributions of predicted stress within concentric (A-B) and non-concentric (C-D) annuli geometries. Modified from [8]. (Right) Confocal images of mammary epithelial cells in a 3D, basement membrane gel of varying stiffness. As the elasticity increases, a more invasive and cancerous phenotype is observed. Modified from [20].

Along with genetic networks and molecular pathways, physical forces and mechanical cues are also being increasingly recognized as important factors which can influence disease progression [17, 18, 19, 20]. For example, stress from a growing tumor mass can contribute to the pinching of blood vessels which are crucial to delivering anti-cancer drugs and nutrients to cells, which then results in amplification of their cancerous behavior [21]. It has also been shown that the mechanics of the

microenvironment surrounding non-tumorigenic mammary epithelial cells regulate their growth [20]. By increasing the stiffness of this microenvironment, cancerous cell behavior is observed via increased invasion of cells into the surrounding microenvironment (Figure 1.3). Consequently, while the tools of molecular biology were traditionally used to investigate the mechanisms behind cancer progression [22], physical forces and mechanical properties have since gained interest as they have a fundamental influence in all aspects of cancer progression, from tumor growth and invasion [18] to metastasis [23].

Given that mechanical forces play such an important role, it is crucial to be able to measure them in living tissues. These measurements, either *in vitro* or *in vivo*, are essential in understanding what mechanical inputs cells are receiving, for example, within different regions of a 3D tissue. Over the past several decades, many methods have emerged to measure mechanics in biological systems. However, it has proven difficult for the majority of techniques to measure mechanical forces locally (*in situ*), in 3D, and in physiologically relevant conditions. These local stresses may give rise to patterns in mechanics which are essential to cellular processes and behavior within 3D tissues, including tumor progression. In this work, I address this need through the use of oil droplets, used as force transducers, which enable the measurement of cell-generated stresses *in situ*, in 3D living tissues.

1.2 Measuring Forces in 3D Tissues

2D cell culturing methods are an excellent platform to study molecular and cell biology, in an environment where biochemistry can be more easily controlled (compared to *in vivo* systems). These 2D monolayer cultures have represented many *in vitro* studies, however, they do not often recapitulate 3D tissue conditions [24, 25] and display important differences from 3D tissues, such as altered cell morphology and gene expression [26]. Due to these differences, this work focused on the measurement of mechanical forces in 3D tissues. Therefore, we only discuss mechanics in the context of 3D multicellular systems in this chapter .

Although mechanics has been shown to play an essential role in biological development and disease progression for several decades, developing techniques to study physical forces in 3D tissues proved to be a challenging task. Despite the inherent difficulty in performing these measurements, advances in technologies such as microscopy and micromanipulation have enabled the investigation of mechanics in 3D tissues. There are now numerous techniques which enable the measurement of mechanical stresses in biological systems in 3D [27, 28, 29], however, it should be noted that these techniques do not enable endogenous stress measurements within living tissues and several require constant contact between an apparatus and the sample.

Micropipette aspiration is a method which has been used to investigate mechanics in 3D tissues such as cell aggregates [30] and even whole embryos [31]. By aspirat-

Method	Length scale	Advantage	Disadvantage
Micropipette aspiration	1-100 μm	Measures both force and mechanical properties *In vitro, ex vivo* and *in vivo*	Apparatus always in contact with sample Global measurements
Parallel plate compression	1-100 μm	Measures both force and mechanical properties	Apparatus always in contact with sample Global measurements
Atomic force microscopy	1-100 μm	Probes mechanics at sub- and supracellular scales *In vitro, ex vivo* and *in vivo*	Apparatus always in contact with sample Limited to surface measurements of 3D tissues
3D traction force microscopy	>5 μm	Physiologically relevant and ease of use	Difficult to obtain straightforward displacement of beads Computationally expensive
Elastic microbeads	>5 μm	Local stress measurements	Used with applied surface stress
Optical and magnetic tweezers	0.1-10 μm	Measures both force and mechanical properties *In vitro, ex vivo* and *in vivo*	Difficult to use *in vivo* Complex calibration
Oil droplets	>5 μm	Local and tissue-scale measurements *In vitro, ex vivo* and *in vivo*	Must control surface chemistry Not able to measure isotropic stresses

Table 1.1: Methods to measure forces in 3D, living tissues.

ing the sample (singe cell, 3D tissue or whole embryo) into the micropipette with a known (negative) pressure, and observing the deformation of the sample shape over time, one can measure mechanical forces from its static response, and mechanical properties from its dynamic response [30,32]. While this method is advantageous due to the measurement of both forces and mechanical properties (e.g. viscoelastic properties), ranging from single cells to tissue-scale studies, the sample must always be in contact with the glass pipette during experimentation, which may disrupt normal development.

Parallel plate compression has also been used to quantify surface tension and mechanical properties of embryonic tissues [33] and cell aggregates [34]. Using parallel plate compression, the sample is squeezed between two parallel plates where typically one of the plates is movable, and connected to a cantilever. This enables studies of static and dynamic compression, by tracking the deformation of the sample over time. As in the case of micropipette aspiration, experiments done by plate compres-

sion bring the tissue sample in contact with the apparatus, and do not enable local stress measurements within the sample.

Atomic force microscopy can be used to both apply and measure mechanical forces, through the use of a calibrated cantilever beam [35]. Measuring the deflection of the beam, which is composed of a material with known mechanical properties, enables precise measurements of mechanical forces [36]. While atomic force microscopy has been typically at subcellular length scales, adaptations of the method have enabled forces at larger length scales (spanning several microns) to be measured [37]. However, much like the previous methods mentioned thus far, atomic force microscopy requires that the apparatus be in direct contact with the sample of interest. Additionally, while suitable for measurements of 3D tissue surfaces, it would not be possible to measure forces beyond the surface with atomic force microscopy.

2D traction force microscopy methods have been extended to enable 3D measurements of mechanical forces [38]. Typically fluorescent beads are embedded within an elastic gel containing a known elastic modulus. Cells apply forces and deform the elastic gel such that the beads move. The bead displacement is quantified and with a known gel elasticity, the stresses applied by the cells can be obtained. This is an elegant and simple method to conduct, however, it is computationally expensive. Furthermore, the samples must be embedded within an external (confining) hydrogel, which does not enable measurements of stress in the absence of confinement.

Both optical tweezers [35, 39, 40] and magnetic tweezers [35, 41, 42] have been used to measure cellular forces and mechanical properties. Optical tweezers use a focused laser beam to trap a bead, which is then tethered to the trap center by a spring-like restorative force. On the other hand, magnetic tweezers use a magnetic field to manipulate small magnetic beads within living cells and tissues. Both techniques enable the measurement of cellular and subcellular forces and mechanical properties. While both methods have been used extensively for *in vitro* studies [35], extending their use to embryonic tissues *in vivo* is difficult because complex calibrations are needed. Moreover, these methods are limited to surface measurements, because the application of forces deep within a 3D tissue is not possible.

A recent study used elastic microbeads to measure how external applied stress propagated throughout tumor spheroids [43]. A surface stress is applied externally to the spheroid via osmotic stress, using Dextran in the outer solution. By applying this surface stress to the 3D tissue, the shape change of the previously inserted beads (with known mechanical properties) enables the stress propagated into the spheroid to be quantified, in response to the surface stress. While this method does enable local measurements of isotropic stress (stress applied uniformly to the microbead) to be measured, it is not performed in the absence of an externally applied stress, thus, endogenous stresses were not measured with this technique.

The aforementioned methods have all provided excellent insight to understand mechanical forces in living tissues, and apply forces to observe the mechanical influence on cellular behavior. With many techniques focused on quantification of 3D mechanics *in vitro*, new methods have emerged (or older methods adapted) to enable the investigation of 3D mechanics *in vivo*. Although researchers have created new approaches to a difficult task, the established methods typically do not allow for quantification of endogenous cell-cell stresses, within 3D tissues.

This thesis focuses on the optimization of a technique which overcomes the aforementioned shortcomings from previously established systems. This technique utilizes microdroplets to measure cell-generated stresses, endogenously in 3D tissues [44]. The method, described in detail in Chapter 2, relies on knowing the curvature of a droplet and its interfacial tension, in order to measure normal anisotropic stresses (stress applied non-homogeneously to the droplet surface).

1.3 Outline of Thesis

The focus of this thesis lies in the optimization of microdroplet methods to enable accurate measurements of stress in living tissues *in vitro* and *in vivo*, in 3D:

1. In Chapter 2, I create droplet sensors to be used as force transducers, from only commercially-available materials, making the previously established method [44]

more accessible. A two-surfactant system controlled the interfacial properties of droplets, while microfluidics were used to generate monodisperse emulsions. Pendant drop tensiometry was used to characterize interfacial properties of different fluorocarbon oils, with both hydrocarbon and fluorocarbon-based surfactants. Flow-focusing, microfluidic devices were used to generate the emulsions. Overall, this system enables accurate measurements of stress both *in vivo* and *in vitro*.

2. In Chapter 3, I use the newly developed droplets to measure endogenous, anisotropic stresses within multicellular aggregates as a function of space and time. This work allowed the first look at measurements of spatiotemporal variations in local, cell-generated stresses due to growth within 3D cell spheroids - a system widely used as model tissues and tumors in a variety of studies. We observed that these stresses do not vary spatially, however, the magnitude increases over time. This temporal increase in stress was found to be dependent on the ability of the droplets to adhere to neighboring cells.

3. Chapter 4 covers collaborative work to synthesize and characterize novel fluorosurfactants. These surfactants were developed in order to provide optimal stabilization of fluorocarbon oil-in-water emulsions. A new synthetic approach enables the creation of fluorinated surfactants with completely non-ionic start-

ing materials, with tunable surfactant geometry. This enabled superior stabilization of fluorocarbon oil-in-water emulsions compared to other systems.

4. In Chapter 5 I discuss final thoughts and potential avenues for further exploration, pertaining to the research conducted in Chapters 2-4.

Chapter 2

Microdroplets to Measure Cell-generated Mechanical Stresses

2.1 Introduction: Oil Droplets to Measure Cell-generated Forces in 3D

Recently, a method was developed to measure cell-generated stresses within 3D multicellular systems using oil droplets [44]. Cell-sized, fluorescently-labeled oil droplets were used as force transducers in living tissues, and measurements of mechanical stress were obtained within tissues both *in vitro* (from cell aggregates) and *ex vivo* (excised embryonic tissue) (Figure 2.1) [44]. Importantly, this technique enabled quantitative measurements of stress, *in situ*, in these 3D tissues.

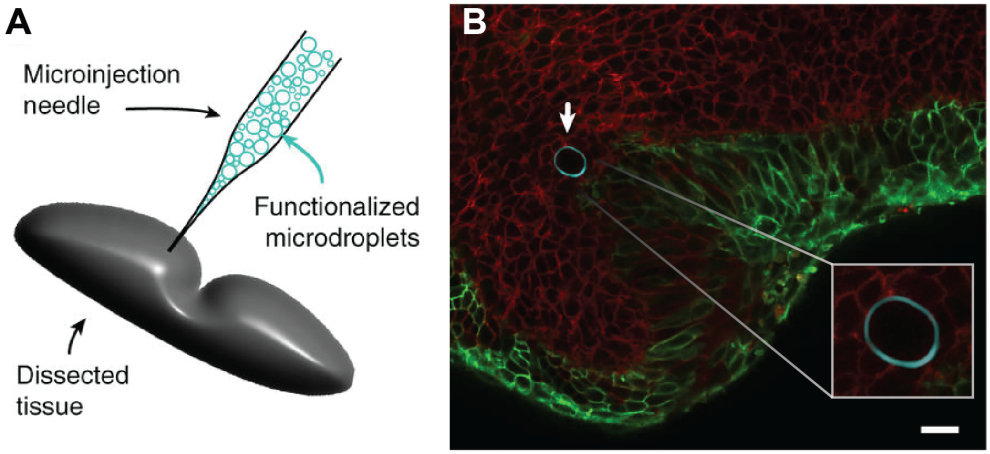

Figure 2.1: Stress measurements in living tissues *ex vivo*. (A) Polydisperse droplets are back loaded into a microneedle, and injected into tissues. (B) Confocal section of a droplet (cyan) embedded within a dissected mouse mandible. Epithelial cells express membrane-localized EGFP (green) and all other cells express membrane-localized tdTomato (red). Scale bar 20 μm. Modified from [44].

The two important parameters one must measure using this technique is the droplet inferfacial tension γ, and the droplet shape, or its mean curvature κ (Figure 2.2). Thus, by imaging the deformation in the shape of droplets induced by normal stresses applied by surrounding cells, and by characterizing the interfacial tension, the droplets may be used as force transducers to measure *anisotropic* stresses (stresses applied non-homogeneously to the droplet surface). Following [44], the anisotropic component of normal stresses $\delta\sigma_{nn}(\theta, \phi)$ is related to the droplet shape and γ via

$$\delta\sigma_{nn}(\theta, \phi) = 2\gamma(H(\theta, \phi) - H_o) \tag{2.1}$$

where H is the local mean curvature and H_o is the average surface mean curvature (H_o=1/R for an undeformed spherical droplet). The stress metric obtained in this way enables the deviation of stress from the isotropic state to be investigated. As mentioned in [44], this techniuqe does not enable the measurement of isotropic stresses, due to incompressibility of the oil droplets used as force transducers. Using this initially developed system, anisotropic stresses were quantified within cellular aggregates of mouse mammary epithelial cells and mesenchymal cells [44].

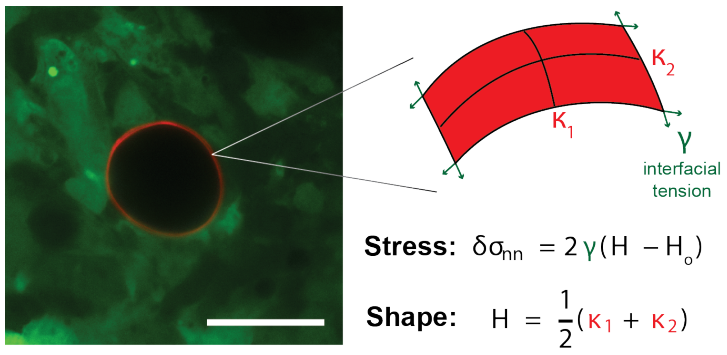

Figure 2.2: Use of droplets as force transducers. (Left) A deformed droplet (red) embedded within a 3D cell aggregate of mesenchymal cells (green). Scale bar 20μm. (Right) Schematic of local droplet interface. To use droplets as force transducers, the interfacial tension γ and curvature κ must be known. H_o is the average surface mean curvature.

This initial study introduced the oil droplets as a proof-of-principle method to measure stresses within living tissues locally in 3D, however, it contained several limitations. There was little control of the droplet surface chemistry, due to a lack of suitable fluorinated surfactants (discussed in more detail in Chapter 4) and a high degree of polydispersity in the droplet size. Poor control over the interfacial tension, which is directly proportional to the desired stresses (Equation 2.1), does not enable accurate measurements of anisotropic stress in the system. Custom co-surfactants were

generated to lower the droplet interfacial tension to enable their use in living embryonic tissues [44], however, this did not enable sufficient control over the interfacial tension in the presence of complex chemical environments with high concentrations of salt and small surface active media, such as that found in cell culture media. This is likely due to the use of surfactants generated from charged starting materials [44], which has been shown to cause changes in the interfacial tension in the presence of reagents typically used in cell culture media [45]. In addition to variations in interfacial tension, bulk emulsification was used to generate the droplets which produced a polydisperse emulsion with a wide droplet size distribution. This complicates the use of droplets as force transducers, due to the difficulty to perform experiments when cells may internalize small droplets - additionally, as the capillary stress increases as its radius decreases, small droplets would provide greater resistance to deformation which would limit their use in systems where cells may apply lower stresses. On the other hand, the presence of very large droplets may perturb the system and can be problematic to embed in various multicellular systems. This limited control over the physical and chemical properties of the droplets, in addition to the use of custom-made surfactants, hindered the practical use of the technique in a variety of systems to measure cell-generated stresses.

The goal of the research conducted in Chapter 2 was to introduce a new system of droplet-based force transducers which is based on only commercially-available mate-

rials, with fully controlled physicochemical properties. To control the droplet interfacial tension and mediate cell-drop interactions, a two-surfactant system was used. This two-surfactant system is more resistant to changes in the droplet interfacial tension in the presence of complex chemical environments found *in vivo* and *in vitro*, containing small surface-active molecules and varying ionic strengths. In order to maintain control over the droplet size, commercially-available, glass-based microfluidic devices were used to generate monodisperse fluorocarbon oil-in-water emulsions. While the current system of droplet-based force transducers boasts controlled properties for accurate measurements of cell-generated stresses, future work is discussed (Chapter 4) to enable facile development of custom-made fluorinated surfactants to further optimize the method and enable long-term stabilization of fluorocarbon oil-in-water emulsions.

2.2 Methods

Preparation and Characterization of bulk Fluorocarbon oil-in-water emulsions

For rapid tests of emulsion stabilization and to ensure proper coatings of droplets were performed, bulk emulsions were generated by hand [46] (Figure 2.3). A 4 mL glass vial was coated with a 0.1% (w/w) BSA solution, rinsed with deionized water

and then 1 mL of DSPE-PEG(2000)-biotin at 0.2 mM final concentration was added. Approximately 100 μL of fluorocarbon oil (either neat or with surfactant, depending on the experiment) was added to the 0.2 mM DSPE-PEG(2000)-biotin solution. The vial was then vigorously shaken by hand (Figure 2.3A) to generate a course emulsion. Afterwards, a pipettor with a 1 mL tip was used to rapidly aspirate and dispense the oil against the glass vial (generating large shear stresses) to narrow the size distribution of the resulting polydisperse emulsion (Figure 2.3B). Since the density of fluorocarbon oils is greater than that of water, the emulsion settles to the bottom of the vial (Figure 2.3C). If large droplets were observed (by eye) shearing with the pipette tip was repeated to generate a finer emulsion. Stability of the resulting emulsion was checked by imaging on an inverted microscope (Figure 2.3D). Filtering of bulk emulsions is done with a 3 μm membrane filter (Sigma-Aldrich, 266574) to further narrow the

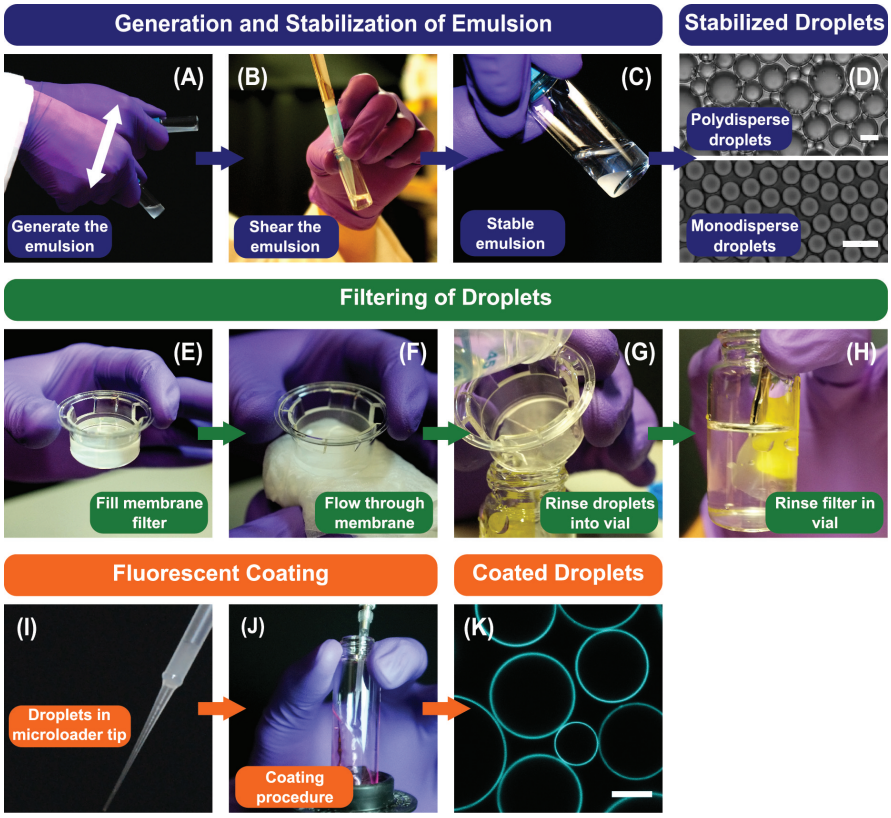

Figure 2.3: Generation and functionalization of droplets via bulk emulsification. (A) Vigorous shaking to generate a bulk emulsion and (B) shearing with a pipette tip to create a finer emulsion. (C) Stable droplets in the vial after generation. (D) Polydisperse and monodisperse droplets, created by bulk emulsification and microfluidics, respectively. (E-H) Filtering droplets by size using a membrane filter (3 μm pore size). (I) Droplets loaded into the microloader pipette tip prior to coating. (J) The fluorescent streptavidin solution is vortexed while droplets are dispensed using a microloader pipette tip. (K) Fluorescent confocal image of a stable, polydisperse emulsion. Scale bars, 25 μm.

wide size distribution resulting from emulsification (Figure 2.3E-H). Droplets were contained in water on top of the membrane filter (Figure 2.3E), and filtered by inducing flow through the pores with a Kimwipe (Figure 2.3F). With a lip in the filter cut, abundant deionized water was used to rinse the droplets into separate vial (Figure

2.3G). Lastly, using tweezers, the filer was rinsed in the vial to recover any excess droplets that remained (Figure 2.3H).

Droplets were further made fluorescent and functionalized with biotinylated ligands to mediate adhesion between the droplet and surrounding cells [46] (Figure 2.3I-K). With many commercially available fluorescent-streptavidin conjugates and because the biotinylated ligand is interchangeable, this system is adaptable to many different experimental conditions, enabling stress measurements in a variety of living tissues. Droplets were placed into a vial of deionized water and rinsed by replacing the water three times in total, to remove excess DSPE-PEG(2000)-biotin surfactant from solution. Droplets were then aspirated using an Eppendorf microloader pipette tip, which was cut (with an inner diameter of $\sim 140\mu$m) to ease the aspiration and dispense of droplets (Figure 2.3I). Since streptavidin has more than one binding site, it should be noted that creating a larger orifice in the Eppendorf tip should be avoided because this will increase the probability of simultaneous dispensing of droplets, increasing the potential that droplets adhere to each other (via the same streptavidin molecule).

To coat them with fluorsecent molecules, the droplets were dispensed into a swirling solution containing 2 μM of AlexaFluor-streptavidin conjugates (Figure 2.3J). Presence of the fluorescent streptavidin conjugate at the droplet interface can be confirmed by imaging the droplets via fluorescence microscopy methods, such as confocal mi-

croscopy (Figure 2.3K). The fluorophore on the streptavidin molecule was tuned based on the experimental conditions where the droplets would be used - AlexaFluor 633 (Thermofisher, A22284) was used for experiments done in cell cultures. The droplets were then stored at 4 $^{\circ}C$ for 1 hour, and subsequently rinsed three times to remove excess AlexaFluor-streptavidin conjugates from solution. For experiments in tooth-mesenchymal cells, the droplets were coated with arginine-glycine-aspartate (RGD) peptides (Peptides International, PCI-3697-PI) at a concentration of 20 μM to enable droplet adhesion to nearby cells [46]. This was done by gently mixing a vial containing the droplets in a solution of the RGD peptides and then incubating them at 4 $^{\circ}C$ for 1 hour. The droplets were rinsed again three times with deionized water prior to use in cell culture experiments. For experiments where we wanted to prevent cell adhesion to the droplet surface, we repeated the same procedure by replacing the ligand with a 5 μM solution of biotinylated mPEG(1k molecular weight) (Creative PEGworks, PLS-2056).

To characterize the interfacial tension of our droplets with multiple surfactants in different environments, pendant drop tensiometry was used (Figure 2.4) [46]. An optical tensiometer (Biolin Scientific, Theta Optical Tensiometer) was used to measure equilibrium interfacial tension values. Fluorocarbon oil droplets (either neat or containing surfactants) were suspended from syringe needles (typically 25 gauge, Jensen Global, JG25-1.0X 50) while immersed within an aqueous media inside of a cuvette

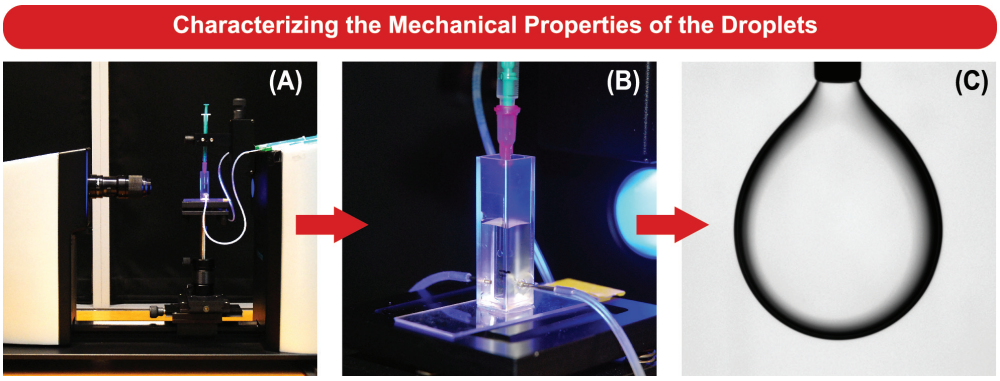

Figure 2.4: Measurement of the interfacial tension using the pendant drop method. (A) Theta optical tensiometer setup. (B) Perfusion chamber for continuous interfacial tension measurements during successive droplet coatings. (C) A pendant drop of FC-70 oil in water.

(BRAND, 759170). Automated software from the tensiometer enabled detection of the interface and calculated (using the Young-Laplace equation) the resulting interfacial tension between the two fluids. Three measurements were taken over several minutes to 0.5 hours, depending on the surfactant concentration used, for all combinations of oil and surfactants to enable average measurements of equilibrium interfacial tension values.

Microfluidics to Generate Monodisperse Fluorocarbon Oil-in-water Emulsions

Many studies take advantage of soft lithography generation of microfluidic devices fabricated from polydimethylsiloxane (PDMS), due to the rapid production and cost effectiveness of the approach. However, PDMS is a naturally hydrophobic polymer, and

is typically used to generate water-in-oil emulsions (here the carrier phase fluorocarbon oil preferentially wets the surface of the channel walls), the inverse of our system. In lieu of modifying the surface chemistry of PDMS-based devices, we utilized commercially available, glass-based (e.g. naturally hydrophilic channel walls) microfluidic devices. Microfluidic devices with a 20 μm channel depth, made from glass (borosilicate), were purchased (Micronit, FC FFDG.2 PACK) to generate monodisperse fluorocarbon oil-in-water (O/W) microemulsions. Droplet generators with a flow-focusing geometry were used, in combination with the Fluidic Connect PRO Chip Holder (Micronit, FC-PRO-CH4515) made to interface with these droplet generators. Syringe pumps (New Era Pump Systems, NE-1000) were used to maintain control over the flow rates. To ensure that the surfaces were sufficiently hydrophilic and to prevent wetting of the droplet phase, the channel walls were coated with a 1% (w/w) solution of bovine serum albumin (BSA). To this end, BSA was flowed through the channels for 30 minutes, followed by a rinse with deionized water (purified through a Milli-Q purification system) by flowing water through the channels for at least 30 minutes, prior to generating droplets. Droplets were generated with a continuous (outer) phase (CP) of 0.2 mM DSPE-PEG(2000)-biotin (Avanti Polar Lipids, 880129) and a disperse (inner) phase (DP) of 2% (w/w) Krytox-PEG(600) fluorosurfactant (RAN Biotechnologies, 008-FluoroSurfactant) dissolved in Novec 7700 oil (3M, 98021248285). To obtain droplets

of 20 μm in diameter the disperse phase flow rate was maintained at 1 μL/min while the continuous phase was typically set in the range of 30-35 μL/min.

For droplet collection, a 4 mL vial was coated with a solution of 0.1% (w/w) of BSA, rinsed, and filled partially with at least 1 mL of fresh deionized water, as detailed in [46]. Tubing from the exit reservoir of the device was submerged into the 4 mL vial, where droplets could be observed (by eye) to sink to the bottom of the vial. It is important to note that lowering the CP flow rate (typically lower than 10 μL/min) will not allow droplets to flow out of the device, and they instead will sit at the bottom of the exit reservoir - this is due to the density of the droplets being approximately double that of water (for Novec 7700 specifically, it is 1.797 times the density of water). Inverting the entire device resolves this issue, however, it complicates the ability to image and monitor droplet generation over time. Once an adequate amount of droplets were collected, tubing was removed from the collection vial, and the syringe pumps were stopped. Afterwards the device was cleaned by removing any leftover BSA or surfactant. Briefly: (1) the channels were rinsed to remove excess BSA or DSPE-PEG(2000)-biotin by flowing deionized water through them at 3 and 1 μL/min (CP and DP, respectively) for 1 hour (2) the channels were rinsed to remove excess fluorosurfactant by flowing Novec 7300 through them at 3 and 1 μL/min (CP and DP, respectively) for 1 hour (3) air was blown through the glass microfluidic device and then it was placed in an oven overnight at 300 $^{\circ}C$. Improper cleaning of devices can cause severe wet-

ting in subsequent experiments when reusing the microfluidic devices, and disrupt or even prevent droplet generation under these experimental conditions. Enabling fluorescence and functionalization of droplets generated via microfluidics follows the same procedure described above, used for droplets generated from bulk emulsification (Figure 2.5A).

2.3 Results and Discussion

Control of Droplet Interfacial Properties

When using droplets to measure cell-generated stresses, the interfacial tension is directly proportional to measured stresses [44]. Thus, it is essential to control and prevent the variation of the droplet interfacial tension potentially arising from changes in ionic strength or other small molecules (e.g. proteins) competing with surfactants for the surface. Being able to control the interfacial tension is also important to be able to use the droplets as force transducers in different systems, such as in multicellular aggregates or different regions within embryonic tissues, where the cellular stresses may vary by orders of magnitude. The originally developed system of droplet force transducers did not enable adequate control over the interfacial tension when using DSPE-PEG(2000)-biotin with custom dodecylamine (DDA) co-surfactants [44].

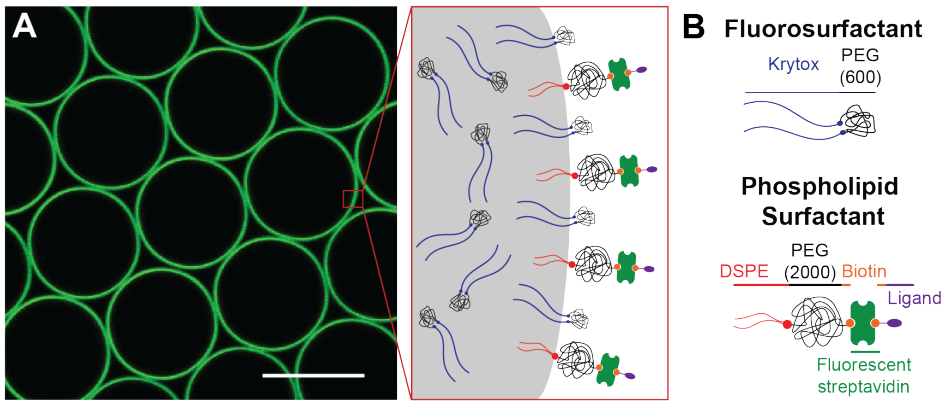

Figure 2.5: Two-surfactant system to control droplet interfacial tension and cell-droplet interactions. (A) Fluorescent (Alexa-Fluor 633) confocal image of monodisperse Novec 7300 droplets coated with the two-surfactant system. Scale bar, 20 μm. (B) Sketch of the two-surfactant system used to stabilize and functionalize droplets: a non-ionic fluorosurfactant (Krytox-PEG) and a DSPE-PEG(2000)-biotin. The functional biotin group enables subsequent coatings of the droplets with fluorescent streptavidin conjugates. A biotinylated ligand to mediate cell-droplet interactions is linked to the streptavidin molecules at the droplet surface.

To enable more independent control over the droplet's interfacial tension and the droplet-cell interactions, we introduced a new surfactant system which uses a commercially-available fluorosurfactant, Krytox-PEG(600) [47] (fluorosurfactant; Figure 2.5B), that controls the interfacial tension and a commercially-available phospholipid surfactant, DSPE-PEG(2000)-biotin (Figure 2.5B), that mediates the adhesive interactions between droplets and cells via streptavidin-conjugated ligands for targeting cell surface receptors. The fluorosrufactant is a non-ionic triblock composed of perfluoropolyether (PFPE) blocks (Krytox) and hydrophilic (PEG) moieties, and is soluble in the fluorocarbon oil phase (droplet; Figure 2.5A). We demonstrated that the interfacial tension can be varied by either changing the fluorosurfactant concentration

(C_{FS}) or by changing the type of fluorocarbon oil used (Figure 2.6). Using pendant drop tensiometry, equilibrium interfacial tension values were obtained for three different commercially-available fluorocarbon oils, specifically Fluorinert FC43, Novec 7700 and Novec 7300.

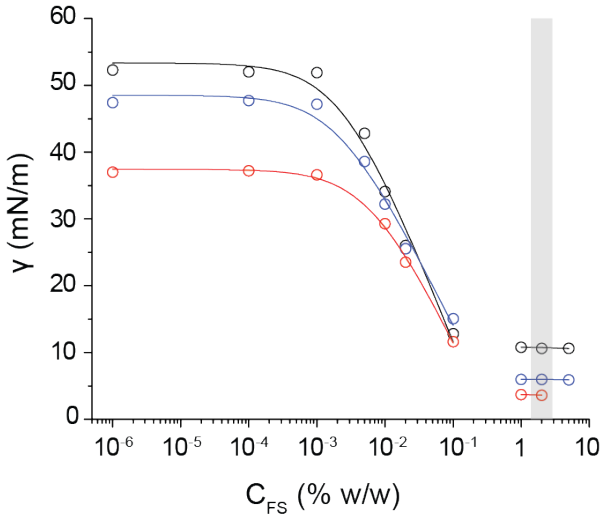

Figure 2.6: Interfacial tension versus fluorosurfactant concentration. Equilibrium interfacial tension of water-fluorocarbon oil (Fluorinert FC43 (black), Novec 7700 (blue) and Novec 7300 (red)) for varying fluorosurfactant concentrations (C_{FS}). The Gibbs adsorption equation was used to fit data in the dilute surfactant regime. Linear fits were performed for data in the saturating regime (non-dilute regime), when the interfacial tension saturates to its minimal value.

Saturating values of interfacial tension were reached as the fluorosurfactant concentration is increased to approximately 1-2% (wt/wt) for the three fluorocarbon oils used. A five-fold decrease in interfacial tension was achieved for Fluorinert FC43 and approximately ten-fold for both Novec 7700 and Novec 7300 (Figure 2.6). Data for equilibrium interfacial tension γ_e versus fluorosurfactant concentration c were fitted (in the dilute regime; Figure 2.6) using the Gibbs adsorption equation [48], namely

$$\gamma_e = \gamma_o - \mathrm{R\,T\,\Gamma_\infty} \ln(1 + \frac{c}{a_L}) \,, \tag{2.2}$$

where γ_o is the interfacial tension of the oil-water interface in the absence of surfactants, R is the gas constant, T is the temperature, Γ_∞ is the saturating surfactant concentration at the interface and $\mathrm{a_L}$ is the Langmuir constant [48]. For saturating fluorosurfactant concentrations (above the dilute regime), in which the interfacial tension γ_e remains largely constant, we used a linear fit. Fitting the data at low (dilute) fluorosurfactant concentrations, yields values of interfacial tension in the absence of surfactants (γ_o = 37.9, 48.3, and 53.5 mN/m for Novec 7300, Novec 7700 and Fluorinert FC43, respectively), the saturating surfactant concentration at the interface (Γ_∞ = 3.51, 4.36, and 4.46 μmol/m^2 for Novec 7300, Novec 7700 and Fluorinert FC43, respectively), and the Langmuir constant, which is related to the energy of adsorption per molecule ($\mathrm{a_L}$ = 6.35, 5.31 and 3.44 μM for Novec 7300, Novec 7700 and Fluorinert FC43, respectively).

The minimum possible interfacial tension achieved with this surfactant system is approximately 3 mN/m (when using Novec 7300), similar to the lowest possible values obtained with previous methods, using DDA co-surfactants [44]. Here, the non-ionic nature of the Krytox-PEG(600) fluorosurfactant enables control over the droplet interfacial tension in environments with small competitive surface active molecules and varying ionic strengths. Measurement of the interfacial tension over a range of ionic strengths, spanning several orders of magnitude, do not substantially change the interfacial tension (Figure 2.7A). By using 2% (wt/wt) fluorosurfactant (in Novec 7700

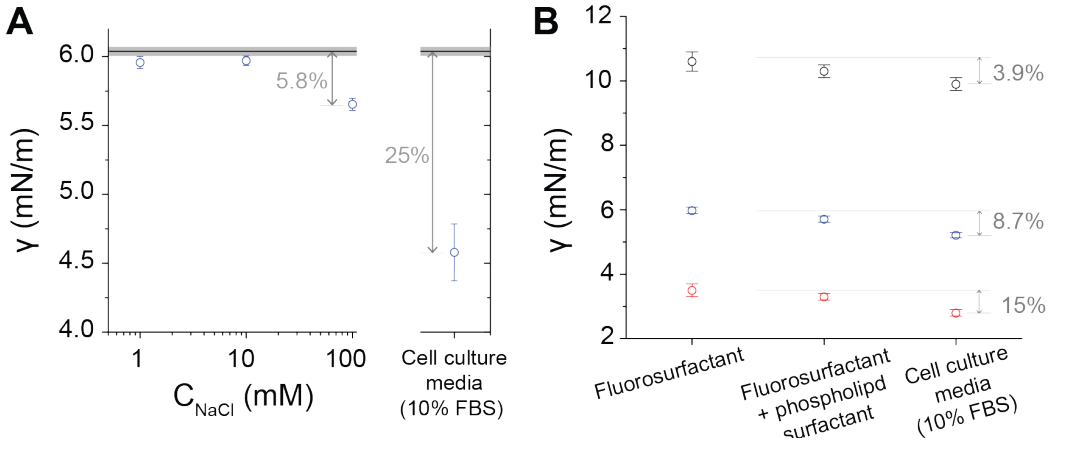

Figure 2.7: Interfacial tension in complex chemical environments. (A) Interfacial tension of Novec 7700 with 2% (w/w) of fluorosurfactant, in the presence of varying concentrations of sodium chloride (C_{NaCl}) (left) and in cell culture media (right). These values are compared to the value of γ in deionized water (gray line). (B) Equilibrium γ values of fluorocarbon oil (same color code as in Figure 2.6) in water with fluorosurfactant alone (2% w/w) and in the presence of fluorosurfactant in the oil and DSPE-PEG-biotin in the water phase. The interfacial tension of the fluorocarbon oil, containing fluorosurfactant and coated with DSPE-PEG-biotin, in cell culture media is also shown.

oil), we observed that only very large concentrations of salt (C_{NaCl}) caused a change in interfacial tension - above ~0.1 M, reducing the interfacial tension by approximately 6%. This slight decrease in interfacial tension may be due to the presence of unreacted, ionic starting materials used to synthesize Krytox-PEG(600) [47]. One study showed that the interfacial tension of interfaces containing only these ionic materials (polar PFPE surfactants; Krytox-FSH) will cause a substantial decrease in the interfacial tension in the presence of phosphate buffered saline (PBS) [48]. To investigate how the fluorosurfactant would behave in the presence of a more complex chemical environment, we measured the interfacial tension of the different fluorocarbon oils with only

the Krytox-PEG(600), in the presence of cell culture media. This cell culture media contains not only PBS and NaCl, but also small surface-active molecules, such as 10% bovine serum albummin (BSA). We observed, by solely using the Krytox-PEG(600) fluorosurfactant at 2% (wt/wt), that the presence of cell culture media decreases the interfacial tension by approximately 25% from the value measured in deionized water (Figure 2.7A). Thus, at saturating surfactant concentrations, the fluorosurfactant alone is able to shield the interface in a complex chemical environment, and offers an improvement over the originally used surfactant system under similar conditions [44].

In order to enable cell-droplet interactions, we coated the droplets with functionalized DSPE-PEG(2000)-biotin surfactants, as previously described [44,46]. In order to investigate the influence of DSPE-PEG(2000)-biotin on the droplet interfacial tension (when the fluorosurfactant is present), we measured the interfacial tension of droplets containing 2% (wt/wt) of Krytox-PEG(600), coated with 0.2 mM DSPE-PEG(2000)-biotin. For each fluorocarbon oil investigated, the interfacial tension drops slightly in the presence of DSPE-PEG(2000)-biotin (Figure 2.7B). To rule out that this could be due to over-saturation of the interface with the competitive, highly surface-active fluorosurfactant, we prepared droplets containing both surfactants and subsequently coated them with AlexaFluor-streptavidin conjugates, which bind to biotin. Fluorescence microscopy imaging of droplets revealed fluorescently labeled droplets, uniformly coated with the fluorophore (Figure 2.5A). We then tested the effect of complex chemical en-

vironments on the interfacial tension of droplets coated with both Krytox-PEG(600) and DSPE-PEG(2000)-biotin by incubating them in cell culture media containing a large concentration (10%) of fetal bovine serum (FBS) (Methods). In the presence of cell culture media the interfacial tension decreases only slightly, with relative changes in interfacial tension before and after addition of the cell culture media for Fluorinert FC43, Novec 7700 and Novec 7300 of 3.9%, 8.7% and 15%, respectively (Figure 2.7B). These results demonstrate that while the interfacial tension is hardly affected by the addition of DSPE-PEG(2000)-biotin, both surfactants work together to largely shield the interface from adsorption of small surface-active molecules in the presence of complex chemical environments like cell culture media. Using this two-surfactant system with different fluorocarbon oils (Fluorinert FC43, Novec 7700 and Novec 7300) leads to the same results, albeit with different interfacial tensions. Therefore, different fluorocarbon oils can be used to achieve a desired interfacial tension of the droplet, and the same two-surfactant system can be used in each oil to keep the interfacial tension constant in different chemical environments. These results demonstrate the versatility of this new, commercial surfactant system, providing low and controlled droplet interfacial tensions even in chemical environments containing high levels of salt and small molecules.

We have developed a controlled and versatile system of droplet stress sensors using only commercially-available components. These new droplet sensors enable the mea-

surement of endogenous, anisotropic stresses within multicellular 3D systems, even in chemical environments with varying ionic strengths or in the presence of small surface-active molecules. Despite a slight decrease of interfacial tension in the presence of cell culture media, the new two-surfactant system largely shields the interface from variations in ionic strength and the presence of small, surface-active molecules. Previous droplet stress sensors [44] relied only on ionic surfactants and their interfacial tension was dependent of the ionic strength of the medium surrounding the droplet. The constant and controlled interfacial tension provided by the new two-surfactant system described herein, as well as the ability to functionalize the droplet surface with virtually any biotinylated molecule, enables the measurement of cell-generated stresses in a wide range of systems.

Control of Droplet Size

Controlling the droplet size is important when using droplets as force transducers to measure cell-generated stresses in multicellular systems. Droplets that are very small are difficult to deform (due to increasing capillary stresses with decreasing droplet size), and may even be internalized by cells. On the other hand, droplets that are too large may disturb normal developmental processes and cell-cell interactions.

Previous work has shown that the optimal droplet size to measure cell-generated stresses is approximately twice the average cell size [44]. As typical cell sizes range

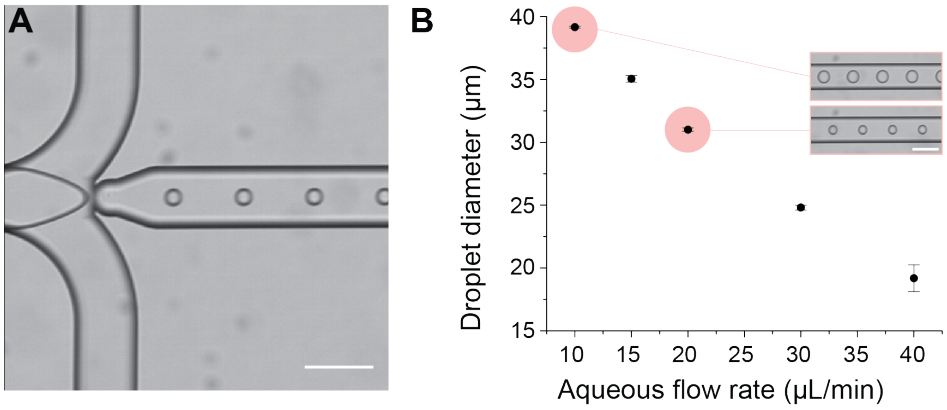

Figure 2.8: Control of droplet size. (A) Droplets generated in glass microfluidic channels, using a flow-focusing device with Novec 7300 oil containing 2% w/w fluorosurfactant as the disperse phase and deionized water with 0.2 mM DSPE-PEG(2000)-biotin as the continuous phase. Scale bar, 100 μm. (B) Droplet size range achieved by varying the continuous flow rate while holding the disperse flow rate fixed at 1 μL/min. Inset shows the difference in droplet size obtained at corresponding flow rates. Scale bar, 100 μm.

between 10-20 μm in many multicellular systems, generation of droplets with diameters between 20-40 μm is desirable. In order to meet this need, we utilized droplet microfluidics to produce monodisperse fluorocarbon oil-in-water emulsions. Using commercially-available, glass microfluidic devices we generated monodisperse, stable fluorocarbon oil-in-water emulsions using a variety of fluorinated oils as the DP: Novec 7300, Novec 7700, and Fluorinert FC 43. The DP contained 2% (wt/wt) Krytox-PEG(600) and the aqueous CP contained DSPE-PEG(2000)-biotin at a 0.2 mM concentration, producing monodisperse droplets through the flow-focusing channel geometry (Figure 2.8A). As a proof of principle, we demonstrate the ability to control the

droplet size by simply changing the CP flow rate, while holding the DP flow rate constant using Novec 7300 oil.

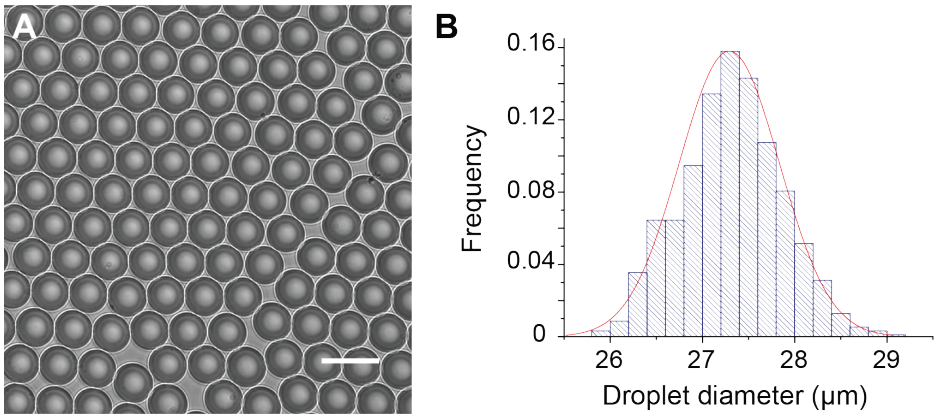

Figure 2.9: Control of droplet size. (A) Brightfield image of a stable, monodisperse emulsion. (B) Droplet size distribution of a Novec 7300 (2% w/w fluorosurfactant, coated with DSPE-PEG(2000)-biotin) with an average droplet diameter: 27.3 $\pm$ 0.5 μm (mean $\pm$ standard deviation).

Varying the flow rate of the CP from 10-40 μL/min produces droplets with an average diameter spanning the range between 20-40 μm (Figure 2.8B). While the droplet size may be varied by changing several parameters [49], typically the flow rate ratio between the CP and DP is changed. Thus, we kept the DP flow rate constant while varying the CP flow rate, to achieve various drop sizes. Droplets generated with this method contain sizes controlled within a 5% relative error (Figure 2.8C), save for cases where the CP fluid velocity is highest, where the device has been shown to produce bidisperse emulsions [50].

As the channel depth is 20 μm, care must be taken to calculate the size of droplets larger than 20 μm in diameter, as they would appear as squashed cylinders during droplet generation. For a squashed cylinder, the total droplet volume V_t is [51]

$$V_t = V_c + V_s \tag{2.3}$$

where V_c accounts for the cylindrical portion of the squashed droplet and V_s accounts for the semicircular portion of the squashed drop volume, which are defined by

$$V_c = \pi d(r - \frac{d}{2})^2 \tag{2.4}$$

$$V_s = 2\pi A_s c \tag{2.5}$$

where d is the channel depth, and r is the squashed droplet radius (Figure 2.10) with

$$A_s = \pi \frac{d^2}{8} \tag{2.6}$$

$$c = r - \frac{d}{2} + \frac{4}{3}\frac{(d/2)}{\pi} \tag{2.7}$$

where A_s being the area of a semicircle and c being the distance from the droplet axis of rotation to the centroid, as shown in Figure 2.10. Knowing the measured squashed

cylinder radius r while the device is generating droplets, and also the channel depth d, V_t may then be used to calculate the (off-chip) diameter of the equivalent spherical droplet.

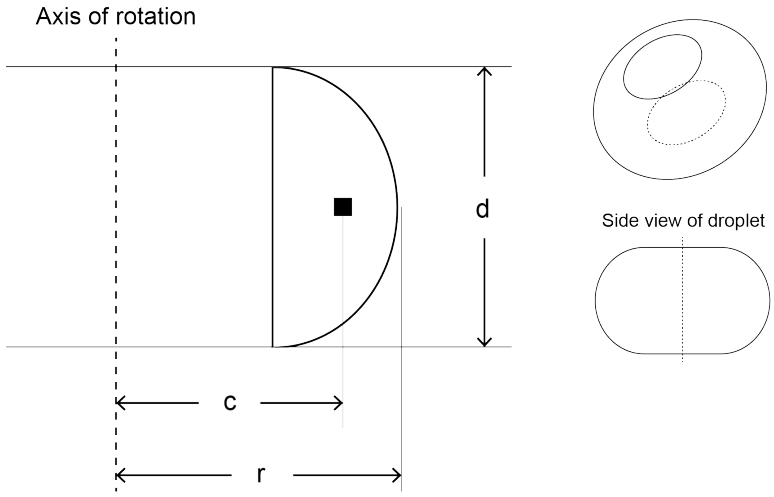

Figure 2.10: Schematic of a squashed droplet. Geometry of a squashed droplet, to correct for the size of a droplet imaged in the microfluidic channel when its diameter is greater than the channel depth d. Modified from [51].

Once droplets were collected as an emulsion, droplet surfaces were coated with fluorescent streptavidin molecules and finally with biotinylated ligands, following the procedures as detailed in [46]. Using confocal microscopy, images of the coated droplets demonstrated the presence of AlexaFluor-streptavidin conjugates (and hence the DSPE-PEG(2000)-biotin molecule) at the surface as previously described above (Figure 2.5A).

2.4 Conclusion

The new, two-surfactant coatings of the droplets and the use of microfluidics for droplet generations allow full control over the relevant parameters. While other studies typically use the fluorocarbon oil as the CP for various experiments [47, 48, 52] (for water-in-oil emulsions), we were able to develop a reliable approach using only commercially-available microfluidic components to generate highly monodisperse fluorocarbon oil-in-water emulsions. Full control over droplet size, in addition to proper shielding of the interface in complex chemical environments, allow these new droplet sensors to be used in a variety of systems as force transducers, either *in vitro* or in *in vivo*.

Chapter 3

Measuring Spatiotemporal Stresses within 3D Spheroids

3.1 Introduction: Mechanics of Cellular Spheroids

2D monolayer cultures have represented many *in vitro* studies, however, they do not often recapitulate 3D tissue conditions [24,25] and display key differences from 3D tissues, such as altered cell morphology and gene expression [26]. Spheroids - spherical aggregates of adherent cells (Figure 3.1) - better mimic 3D tissues than traditional monolayer cultures and maintain important cell-cell and cell-matrix interactions [53]. Furthermore, chemical gradients established within these 3D aggregates of cells (typi-

cally larger than 150-200 μm in diameter) make them suitable models of tumors, which are typically subjected to inner hypoxic regions and proliferative gradients [54, 55].

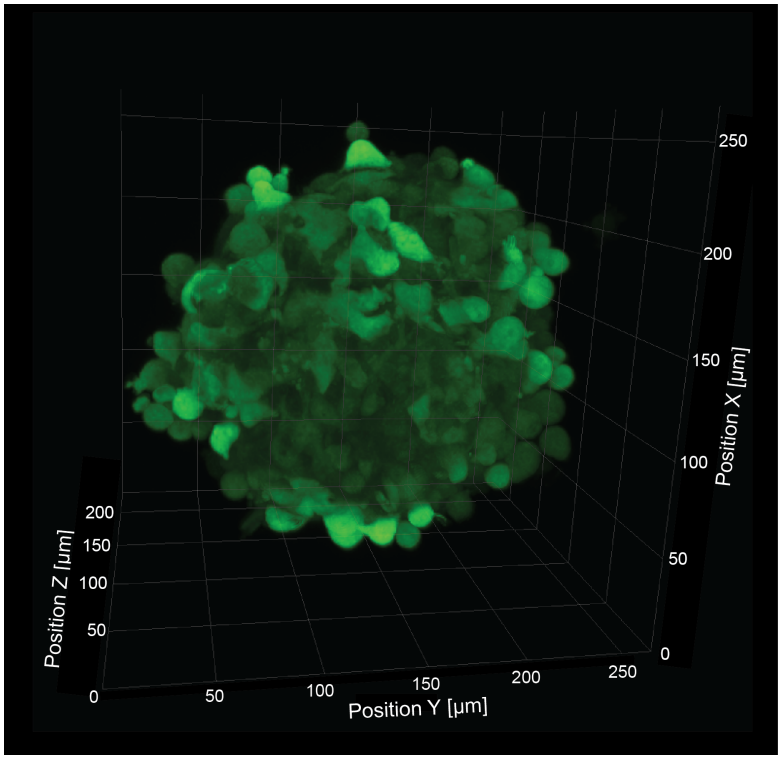

Figure 3.1: 3D cell spheroid. Maximum intensity projection of a mesenchymal cell spheroid, imaged with confocal microscopy. These aggregates of GFP-positive cells better mimic 3D tissues than traditional monolayer cultures.

The application of external forces as well as changes in the mechanical properties of the surrounding microenvironment can strongly influence cell behavior in 2D culture systems [14, 16, 56, 57, 58], and in 3D tissues during development [59, 60, 61] and disease progression [17, 18, 19, 20]. Many studies have focused on the role of the microenvironment external to the multicellular aggregate, however, the endoge-

nous stresses which build within multicellular aggregates remain unknown. Stress variations within cellular spheroids have been suggested to exist [62, 63], but not directly observed. To infer these forces, previous work estimated stress levels within tumors by physically cutting excised tumors, and using the resulting tissue deformation along with a mathematical model [64]. Compressive stresses within murine tumors were estimated to range from 0.37-8.01 kPa using this method. Other methods used less invasive approaches to measure the maximum stress generated by cancerous cell spheroids. The resistance to spheroid growth via confinement in either elastic microcapsule [65] or gels [66, 67], in addition to osmotic pressure [6] (applied to the surface of the aggregate) has been used to measure the bulk mechanical stresses that spheroids apply to their surrounding environment. A recent study used elastic microbeads to measure the influence of mechanical compression on the propagation of isotropic stresses within tumor spheroids [43]. While this work investigates the effect of confinement and external compression on mechanical stresses, the spatiotemporal variation of endogenous stress during aggregate growth and compaction remained unknown. The goal of this research was to utilize the controlled droplets, discussed in Chapter 2, to investigate how stresses within multicellular aggregates change spatially and temporally, as the aggregates grow and compact over time.

3.2 Methods

Cell Culture and Spheroid Formation

To generate 3D aggregates of cells, tooth mesenchymal (TM) cells (a kind gift from Dr. Tada Mammoto; Ingber lab, Wyss Institute for Biologically Inspired Engineering at Harvard), isolated from mice tooth rudiments from day 10 post-fertilization embryos were used. The TM cells were transfected with green fluorescence protein, expressed in the cytoplasm. Standard aseptic cell culture techniques were used to maintain cultures of TM cells: the cells were grown in Dulbecco's Modified Eagle Medium (DMEM) supplemented with 10% fetal bovine serum (FBS) and 1% Penicillin Streptomycin (Pen-Strep), at 37 $^{\circ}C$ with 5% CO2. Subcultures were performed in T25 flasks with at least 5 mL of cell culture media, which was replenished every other day. Cells were passaged once growth reached 70-80% confluence, and each subculture was always passaged less than 15 times. To ensure cell seeding at a specific density, cells were counted using a hemocytometer. It was determined that seeding between 0.25-1x10^6 TM cells in a T25 flask, with 5 mL of cell culture media, maintained an average cell doubling time of approximately 27 $\pm$ 2.4 hours.

While spheroid generation may be done using several methods [54, 68], we followed standard protocols using non-adhesive, round-bottom wells. These wells are typically coated in order to promote cell-cell interactions, while prohibiting cell-surface

interactions, encouraging spheroid formation. Many vendors supplied plates containing round-bottom wells (each coated with some proprietary surface modifications) however, testing with TM cells revealed that using round-bottom wells, coated with a biologically inert hydrogel to prevent cell attachment (Corning, 7007), worked best to repeatedly generate single spheroids of a controlled size. Due to the difficulty from imaging deep into large 3D tissues via confocal microscopy, we aimed to generate spheroids that were approximately 200 μm in diameter. As expected, the size of the resulting spheroid depends on the initial cell seeding number per well. To this end we seeded different densities of cells per well, and measured the aggregate size at different time points, to investigate the optimal seeding cell density.

The range of 10^2-10^5 TM cells per well was investigated, checking aggregate size from 24-96 hours (Figure 3.2). From these results, we seeded 10^3 cells/well into round-bottom wells for experiments to measure stress with droplets. Cell suspensions were dispensed into wells with 200 μL of cell culture media and allowed to incubate at 37 $^{\circ}C$ with 5% CO2. To ensure that cells received fresh media, the cell culture media was replenished every other day by removing 100 μL of old media from each well, and adding 100 μL of fresh media.

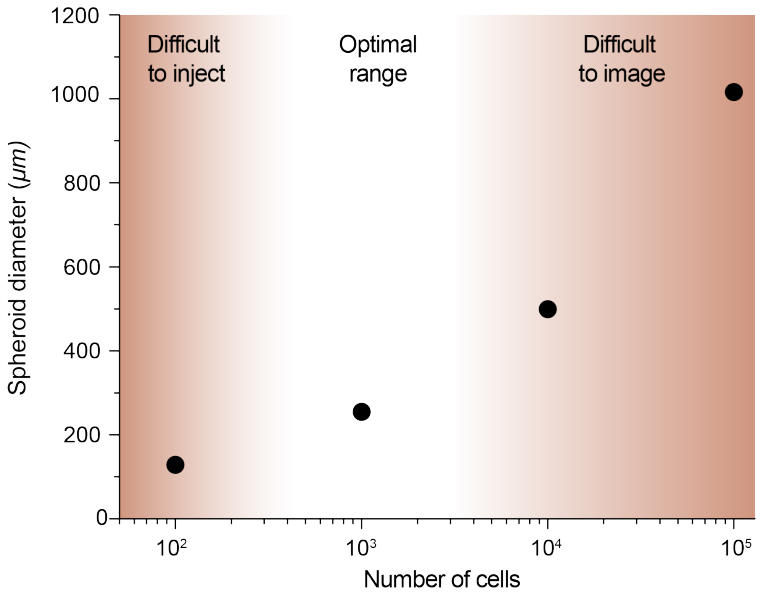

Figure 3.2: Spheroid size versus cell number. Spheroid diameter plotted for an increasing number of cells seeded per well in the desired low-adhesion, round-bottom well plate. Seeding below 10^3 cells per well does not produce a large enough aggregate to inject into, while spheroids above 10^3 cells per well may cause difficulty in imaging in 3D via confocal microscopy

Droplet Embedment within Spheroids and Imaging

Following the methods established in [44], droplets (functionalized with RGD peptides for targeting integrin receptors on the cell surface) and TM cells were initially mixed together by different means to attempt to embed the droplets within the aggregates: (1) suspensions of cells containing droplets were mixed together manually (by hand and via vortex mixing) for approximately 1-2 minutes prior to seeding the mixture into round-bottom wells and (2) droplets were seeded into the wells at different time points, after cells had been allowed to aggregate over various time points - in this

method, droplets were added at various time points after initial cell seeding over 1-24 hours. These methods proved unsuccessful, as it was never observed that spheroids of controlled size could be generated with droplets embedded within. While centrifugation was used to enable droplet embedment in [44], this method does not enable adequate control over the spheroid size, and the influence of centrifugation on the mechanics of the spheroid remains unclear [69]. Thus, we sought to use microinjection of droplets into aggregates in order to introduce single droplets into aggregates, to minimize the disturbance of natural aggregate growth and compaction.

To embed droplets between cells within the aggregates in a reliable manner, a modification to standard microinjection techniques was used. At 16 hours after initial seeding into round-bottom wells, loose TM cell aggregates were transferred from the round-bottom wells into a glass bottom microwell dish (MatTek, P35G-0.170-14-C) with at least 2 mL of cell culture media. Droplets prepared from Novec 7700 oil were placed into the microwell dish, next to the aggregates. These droplets were prepared with AlexaFluor(633)-streptavidin conjugates and functionalized with biotinylated RGD peptides to mediate adhesion to the TM cells. Utilizing a Pico-Liter Injector (Warner Instruments, PLI-100A), a negative pressure was applied to a blunt glass microneedle with an outer diameter of 20 μm. Bringing the tip of the needle close to a droplet partially intakes the droplet into the needle. It is worth noting that droplets smaller than 20 μm in diameter will be sucked up into the microneedle, rather than

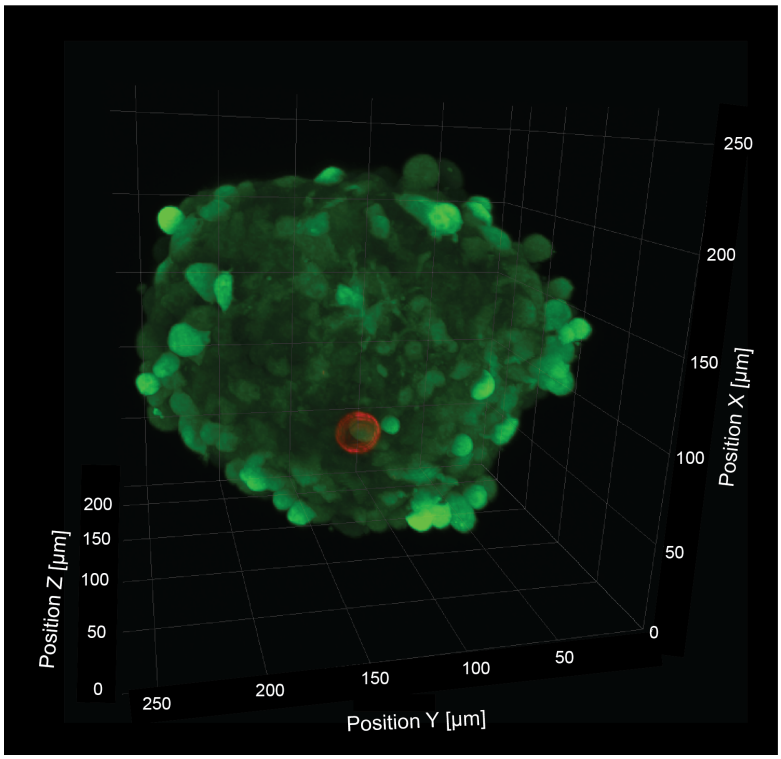

Figure 3.3: Droplet embedded within 3D cell spheroid. Maximum intensity projection of a mesenchymal cell spheroid (green) at 48 hours post-formation, containing a single droplet (red).

be held at the tip. For this reason, we changed the size of the droplets and found that droplets with a diameter between 21-23 μm work best under these conditions. The droplet held at the tip of the microneedle was brought into the aggregate via a small hole made previously with the microneedle. Once inside, the negative pressure was released and the microneedle was removed, leaving the droplet embedded within the aggregate. After injection, aggregates containing droplets were transferred back to the round-bottom wells and incubated at 37 $^{\circ}C$ with 5% CO2 for at least 8 hours be-

fore imaging. Injection of droplets at 16 hours after initial seeding into round-bottom wells enabled stresses to be measured at 24 hours, after the eight-hour incubation period. Injection at this early time point does not allow for stress measurements to be performed at later time points (usually more than 48 hours in our experiments) due to diminishing fluorescence at the droplet surface. To avoid this issue and enable measurement of stresses at later time points, specifically 48 and 60 hours in our experiments, an additional droplet injection point was added at 40 hours.

3D images of droplets were obtained via confocal fluorescence microscopy (Zeiss, LSM 710) and confirmed that droplets remained embedded within spheroids (Figure 3.3). To this end, TM aggregates were transferred back to microwell dishes containing approximately 2 mL of cell culture media via glass pasteur pipettes. 3D fluorescent images of droplets were obtained using a 40x water immersion lens, while the confocal incubation chamber maintained the temperature at at 37 $^{\circ}C$ with 5% CO2. Single droplets were imaged at a time for the measurement of curvature. To avoid the issue of apparent deformation from droplet movement during imaging, the conditions were optimized to image the droplet as fast as possible, at reasonable resolution for reconstruction of curvature: XY resolution was maintained at 256 x 256 and the droplet was imaged in 1 μm slices (Figure 3.4A) simultaneously for two channels (one for the droplet, one for the cells), resulting in an overall imaging time of approximately 30 seconds. To determine the spatial location of droplets within aggregates, whole-

aggregate images were taken: XY resolution was maintained at 256 x 256 and the entire aggregate was imaged in 5 μm slices simultaneously for both the droplet and cell channels. To image droplet movement over time in 3D, aggregates were placed in custom round-bottom wells made from 1% agarose. The agarose was heated until it became a liquid, poured into a microwell dish and then a PDMS mold (containing features to create the wells) was placed on top. Light pressure was applied to the PDMS mold to create wells closer to the bottom of the microwell dish to avoid the chance that aggregates and droplets would be out of the working distance of the objective. The microwell dish was then sealed with parafilm and stored at 4 $^{\circ}C$ for a minimum of 30 minutes. Approximately 2 mL of pre-warmed cell culture media was dispensed into the microwell dish prior to transferring aggregates into it for imaging. For tracking drop movement over time: XY resolution was maintained at 256 x 256 and aggregates were imaged in 5 μm slices every 15 minutes.

Image Analysis and Droplet Reconstruction

To determine the spatial location we used Imaris 3D rendering software (Bitplane). Briefly, surface models of both the droplet and aggregate were generated and the droplet center was located. From this, the minimal distance between the droplet center and the nearest point on the aggregate surface X_s was determined. From this

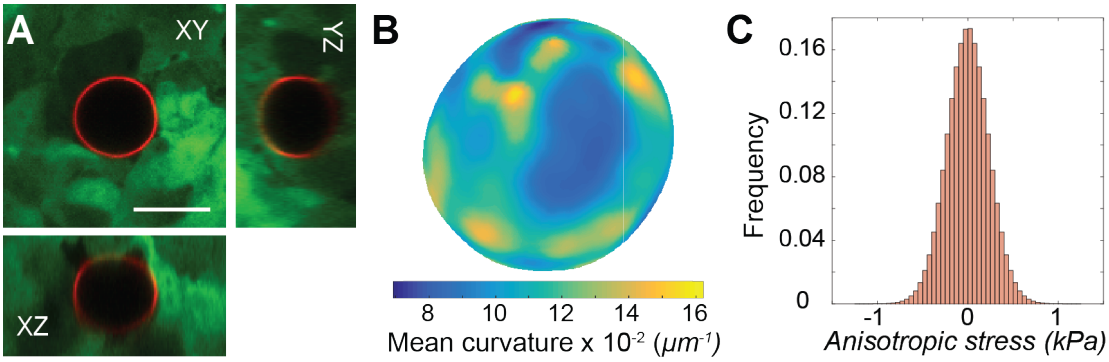

Figure 3.4: Droplet imaging and 3D reconstruction to measure anisotropic stresses. (A) Three planes of a confocal image from a droplet coated with Alexa-Fluor 633 streptavidin (red) and RGD peptides, embedded within a 3D cell aggregate of tooth mesenchymal cells (green). Scale bar, 20 μm. (B) Mean curvature map of the droplet's surface obtained from 3D reconstruction of confocal images. (C) Distribution of measured values of anisotropic stresses for a single droplet.

surface model, the volume of the aggregate was computed, and the aggregate radius (assuming a spherical aggregate shape) was then determined.

A custom Matlab algorithm was used to perform 3D surface reconstruction from confocal images of the droplets (Figure 3.4B,C) [70]. The droplet surface is located and described by a point cloud. This point cloud is used to calculate the mean curvatures locally, via standard differential geometry. To reduce high-frequency noise in images prior to determination of curvature values, we employed both steerable and median filters.

3.3 Results: Spatiotemporal Stress Measurements within 3D Spheroids

Spatial Stress Measurements

Injecting droplets at different locations within many aggregates makes it possible to obtain a spatial map of the stresses of interest. Droplets were prepared with AlexaFluor (633)-streptavidin conjugates and functionalized with biotinylated RGD peptides to target cell integrin receptors. This enabled the investigation of stresses both tensile in nature, and compressive. To obtain the stresses on the droplet surface: (1) the droplets were imaged in 3D via confocal microscopy and their surface was reconstructed (2) the local mean curvature H was calculated over the entire droplet surface (3) the local normal anisotropic stress σ_{nn}^{A} was quantified by measuring the difference in normal stresses between a pair of points ($\vec{x}_1$ and $\vec{x}_2$) on the droplet surface: $\sigma_{nn}^{A}(\vec{x}_1, \vec{x}_2) = \sigma_{nn}(\vec{x}_1) - \sigma_{nn}(\vec{x}_2)$ (Figure 3.5).

A local normal force balance at the droplet surfaces provides a relationship between the normal surface stress applied to the droplet σ_{nn} and the induced deformations which are characterized by the mean curvature $H(\vec{x})$ via:

$$\sigma_{nn}(\vec{x}) = -P + 2\gamma H(\vec{x}) \tag{3.1}$$

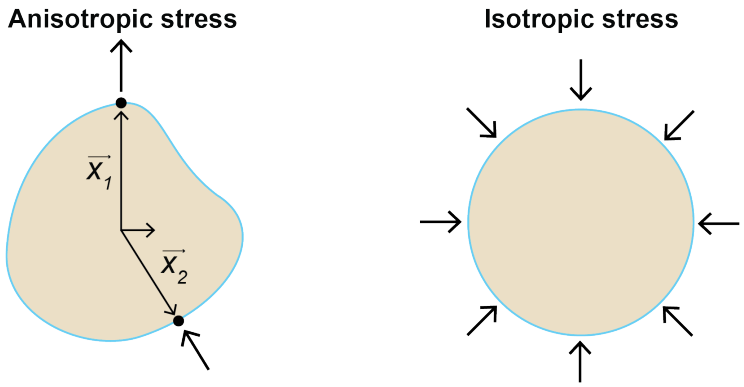

Figure 3.5: Illustration of anisotropic versus isotropic stress. Sketch showing the definition of anisotropic stresses as the difference in normal stresses between two points at the droplet's surface, each associated with a different spatial direction. While not measured with droplets herein, a sketch depicting isotropic stresses is also shown for clarity.

where P is the isotropic pressure and γ is the droplet interfacial tension. It should be noted that we are not able to measure the isotropic pressure due to incompressibility of the droplet (Figure 3.5). Thus, using 3.1, we define the anisotropic stress as

$$\sigma_{nn}^{A}(\vec{x_1}, \vec{x_2}) = 2\gamma[H(\vec{x_1}) - H(\vec{x_2})] \tag{3.2}$$

which depends on the difference in curvature between the two points $\vec{x_1}$ and $\vec{x_2}$,

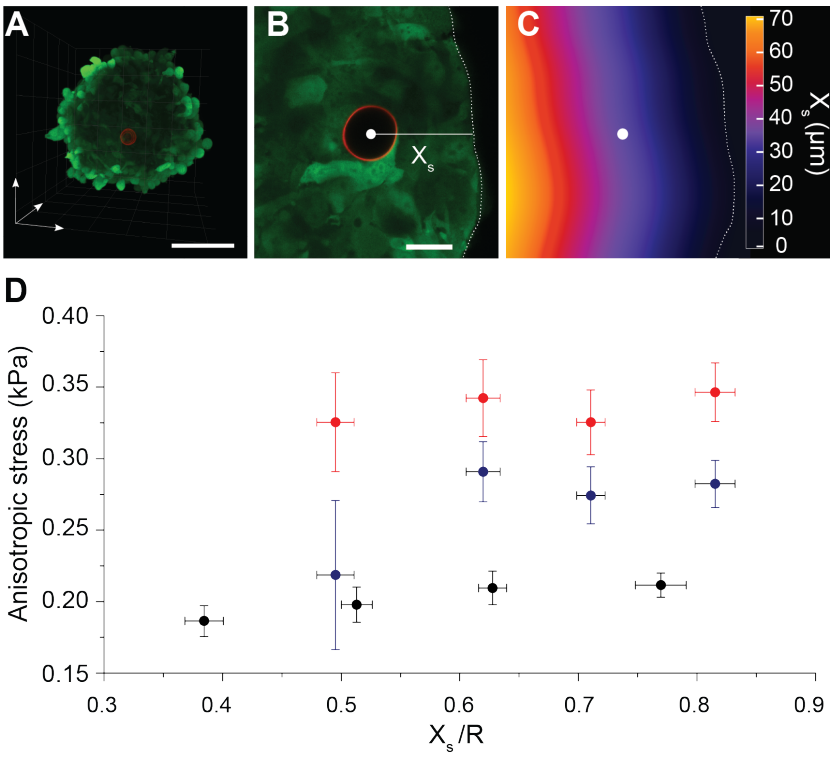

Figure 3.6: Spatial variations in endogenous cellular stresses within 3D cell aggregates. (A) Maximum intensity projection of a single droplet (red) within a 60 hour tooth mesenchymal cell aggregate (green). Scale bar, 100 μm. (B-C) Definition of X_s as the closest distance of the droplet center (white circle) from the aggregate's surface (dashed line). Scale bar, 20 μm. (D) Spatial variation in anisotropic stresses within tooth mesenchymal cell aggregates at 24 (black; N=30), 48 (blue; N=28) and 60 (red; N=24) hours (N = number of aggregates). For each time, data points were binned into four groups. Data points and error bars in each bin correspond to mean $\pm$ s.e.m of anisotropic stress and X_s. The average aggregate radii for 24, 48, and 60 hours are 98.2 $\pm$ 5.7, 103.7 $\pm$ 5.8 and 110.2 $\pm$ 6.5 μm, respectively (mean $\pm$ s.d.).

and the droplet interfacial tension. The droplets, using Novec 7700 oil, have an interfacial of 5.2 $\pm$ 0.1 mN/m in cell culture media (Figure 2.7B). Using Eq. 3.2, we obtain the distribution of anisotropic stresses for all pairs of points on the droplet surface (Figure 3.4C), and use its standard deviation as the metric of the magnitude of the anisotropic

stress measured at different points within the aggregate. Notably, the metric of stress reported herein is different than that reported in [44]; while we now report the difference in normal stress at points $\vec{x_1}$ and $\vec{x_2}$, the metric reported in [44] focused on the deviations in normal stress from the isotropic state.

For both spatial and temporal stress measurements, RGD-coated droplets with an average diameter of 21 ± 1 μm were embedded within aggregates and imaged at time points of 24, 48 and 60 hours (post initial cell seeding). We report the variation of stress as a function of space by defining X_s, the minimal distance of the droplet center from the aggregate surface (Figure 3.6B), obtained from the contour plot of distance from the aggregate's surface (Figure 3.6C). The magnitude of the anisotropic stresses measured varies weakly with spatial location within the aggregate (Figure 3.6D), changing by only about 10% between measurements closest to the surface and those closest to the center. As observed in Figure 3.6D, the spatial range of the measured stresses changes over time. This is due to droplet movement towards the aggregate center over time (discussed below).

Temporal Stress Measurements

Although there was a weak relationship between the measured anisotropic stresses and spatial location within the aggregate, it is evident (also from Figure3.6D) that the magnitude of anisotropic stresses increase considerably over time (Figure 3.7A). Due

to the insignificant spatial dependence, we averaged all data at each time point to determine the temporal variation in cell-generated anisotropic stresses, over the entire aggregate.

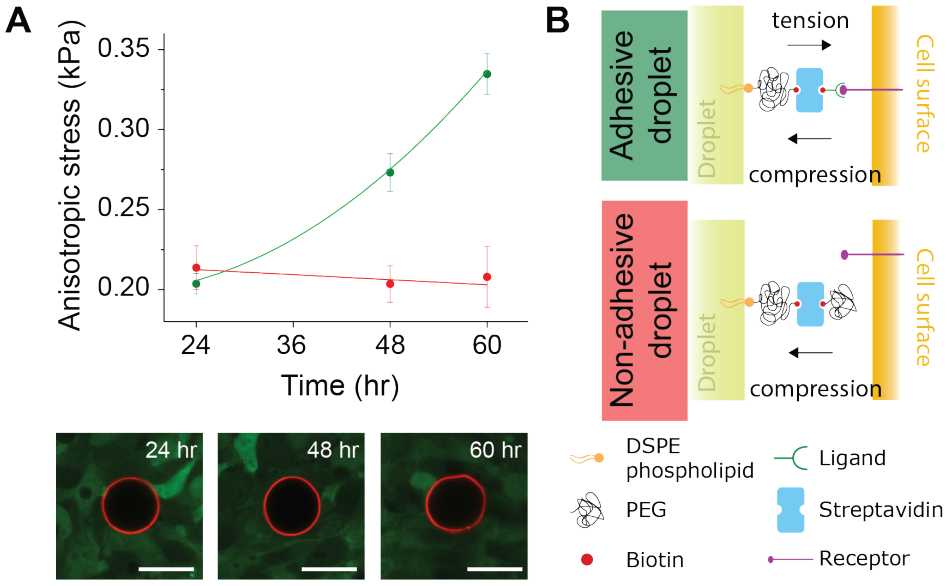

Figure 3.7: Temporal evolution of average cell-generated stresses within growing 3D aggregates. (A) Average anisotropic stresses for tooth mesenchymal cell aggregates at 24, 48 and 60 hours (top), measured with droplets coated with RGD peptides (green) or mPEG (red) to quantify compressive and tensile stresses (see panel B). Confocal sections of RGD-coated droplets (red; surface label) embedded between cells (green) of the aggregate at different time points are shown. Scale bars 20 μm. For 24, 48 and 60 hours, N = 30, 30, and 24, respectively, for droplets coated with RGD peptides, and N = 6, 5, and 5, respectively, for droplets coated with mPEG (N = number of aggregates). (B) Schematic representation of adhesive and non-adhesive droplets to investigate tensile and compressive stress contributions.

The magnitude of the stress increases from approximately 0.2 kPa to 0.35 kPa from 24 to 60 hours, as the aggregate grows and compacts. This increase in droplet deformation (e.g. stresses) over time is directly visible when imaging via confocal microscopy (Figure 3.7A, bottom). Furthermore, to investigate the nature of this in-

crease in stress over time, we hindered adhesive interactions between the cells and the droplets by coating their surface with methoxypoly(ethylene glycol) (mPEG) (Figure 3.7B). Whereas RGD-coated droplets enable measurement of both tensile (pulling) and compressive (pushing) stresses, droplets coated with mPEG solely measure compressive stresses (Figure 3.7A,B). Our results suggest that the variation in anisotropic stress over time is due to the ability of the droplets to adhere to neighboring cells, and that the magnitude of the compressive anisotropic stress remains constant.

Droplet Flow within Spheroids

As observed in Figure3.6D, the spatial range of measured stresses changes over time from 24 to 60 hours. Droplets were observed to move towards the center of the aggregate over time (Figure 3.8A-C), which prevented the measurement of stress close to the aggregate periphery.

Imaging during growth and compaction from 48 to 60 hours, we were able to track the trajectory of droplets over time in 3D within the aggregate. In each case, the droplet moves towards the center (Figure 3.8A) of the aggregate while the aggregate grows. Droplets were observed to move towards the aggregate center with an average speed of 1.2 ± 0.3 μm/hr while the aggregate grew over time (Figure 3.8B) at an average radial speed of 0.38 ± 0.03 μm/hr (Figure 3.8C).

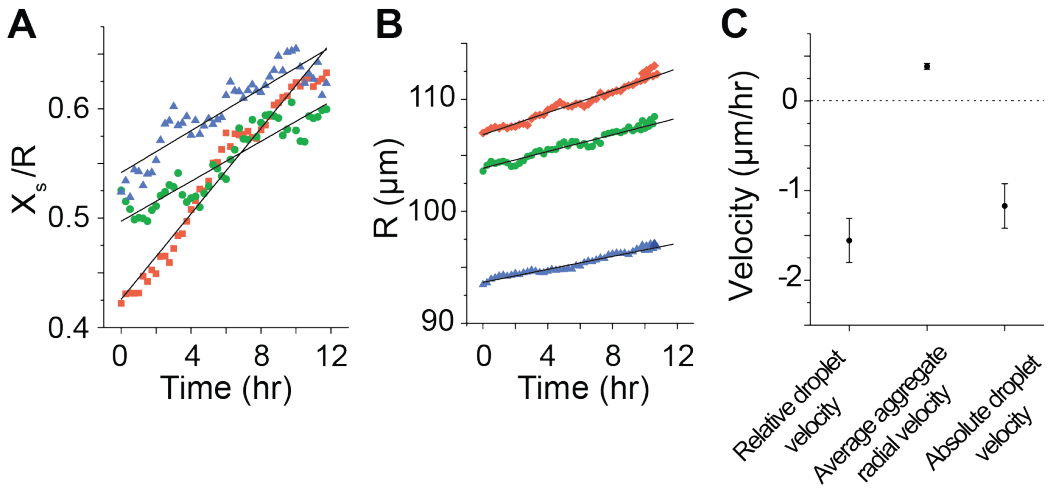

Figure 3.8: Droplet movement within 3D tooth mesenchymal cell aggregates. (A-C) Temporal evolution of droplet position (A) and average aggregate radius, R, (B) for three different aggregates, each containing a single droplet, over 12 hours (from 48-60 hours). (C) Average droplet velocity relative to the aggregate's surface ($-dX_s/dt$), average aggregate radial growth velocity (dR/dt) and also the absolute droplet velocity ($-dX_s/dt + dR/dt$). Values reported represent average $\pm$ standard error of the mean.

3.4 Discussion

Using the new system of droplets as force transducers, we were able to measure endogenous, anisotropic stresses within multicellular aggregates. Both spatial and temporal changes in these stresses were measured within multicellular aggregates. This work allowed the first glance at measurements of spatiotemporal variations in cell-generated stresses within 3D cell spheroids, a system widely used as model tissues and tumors in numerous studies. Our results reveal that over 24-60 hours, the magnitude of anisotropic stress within the aggregate does not strongly vary as a function of spatial location (Figure 3.6D). Comparing the anisotropic stresses obtained from mea-

surements either with or without ligands targeting integrin receptors demonstrates that cell-generated pulling stresses increase over time, as the aggregate continues to grow and compact (Figure 3.7A). This is consistent with previous work which shows that integrins mediate strong adhesion between mesenchymal cells in 3D tissues [71]. The nature of this time-dependent increase in cellular stress may be due to the fact that cells are not able to transmit forces through integrin receptors in loosely-associated aggregates at early time points (24 hours) compared to later time points (after 48 hours). However, the increase in stress could also be due to several other mechanisms, including a mechanical response due to increased cell-cell contacts, increased levels of extracellular matrix, or perhaps due to changes in the mechanical properties of the microenvironment within the cellular aggregate. For these reasons we do not claim that the forces are solely caused by integrin-mediated adhesion between the cells and the drops.

Although no other work has measured endogenous stresses within multicellular aggregates, several studies have estimated the isotropic stress generated by an entire growing aggregate [65, 66]. Tumor spheroids confined within elastic microcapsules generated an isotropic stress of approximately 2 kPa [65], while stress levels within spheroids grown in agarose gels (of varying stiffness) were estimated to be in the range of 3.7-16 kPa [66]. These values are larger than the average anisotropic stress we report herein, however, the difference in the stress metric reported should be noted:

these studies investigate the isotropic, bulk stress applied by the entire aggregate on their surrounding whereas we focus on measurement of the local, cell-cell generated anisotropic stresses in the absence of confinement (Figure 3.5). A recent study has used elastic microbeads to measure spatial variations in isotropic stress, transmitted through the aggregate via an osmotic pressure applied to the surface of tumor spheroids [43]. After applying a stress of 5 kPa to the surface, the isotropic stresses within the spheroid ranged from <1 to 4 kPa, from the periphery to the aggregate core. In contrast to the measurements reported herein, which quantify the spatiotemporal variations in the endogenous anisotropic stresses at the cellular scale (Figure 3.5), the measurements described in [43] correspond to the supracellular, isotropic stresses measured within the aggregate in response to an applied external stress.

The spatial range of measureable stresses changes slightly with time because droplets move towards the aggregate core (Figure 3.8), preventing measurements of stresses close to the aggregate's surface at later times. The existence of inward movement of droplets is consistent with previous observations of core-directed internal flows [72, 73, 74]. These flows are thought to be generated by spatial segregation of cell proliferation and death within the aggregate: cell proliferation occurs preferentially at the surface of the aggregate, whereas cell death occurs predominantly at its core, generating a net flow of cells towards the aggregate center [72,73,74]. In all cases, we observed the droplets to move inward, towards the aggregate's core (Figure 3.8A), while the ag-

gregate radius R increased over time (Figure 3.8B). Droplets moved inward with an average speed of 1.2 $\pm$ 0.3 μm/hr, while aggregates grew at an average radial speed (dR/dt) of 0.38 $\pm$ 0.03 μm/hr (Figure 3.8C).

3.5 Conclusion

By investigating mechanical stresses within multicellular spheroids, widely used as model 3D tissues and tumors, we can help understand how mechanics influence cell behavior in 3D multicellular environments. The use of novel tools such as droplet-based probes or elastic microbeads can compliment cell and molecular biological studies to provide an insight on how physical quantities correspond with molecular cues in 3D multicellular environment. Such tools can be used to investigate mechanical cues in developing embryos and also for studying the role of mechanics in tumor progression.

Chapter 4

New Fluorosurfactants for Stabilizing Fluorocarbon Oil-in-water Emulsions

4.1 Introduction: Fluorinated Materials

Fluorinated materials, in particular for emulsions generated or stabilized with a fluorinated component, have been investigated for their use in numerous applications [75], including drug delivery [76, 77, 78, 79], biomedical imaging [80, 81, 82], and also in the use of droplets as force transducers in living tissues [44]. Most notably, fluorocarbon (FC) oils have been utilized as the dispersed phase in an emulsion to act

as artificial oxygen carriers (AOCs) or "blood substitutes," due to their ability to dissolve oxygen [75, 83, 84, 85] better than most solvents. In the 1960's, the ability of FC oils to dissolve oxygen was demonstrated in unique experiments: Clark and Gollan immersed rats within a solution of oxygen-saturated, FC oil at atmospheric pressure and showed that they could live and breathe within the fluid [86]. These oils were also found to support regular contraction of excised rat hearts *ex vivo*, when perfused with an oxygen-saturated FC oil and diluted blood [87]. Altogether, these experimental findings supported the use of FC oils in the biomedical field, and sparked the interest of using them as AOCs.

The unique properties of fluorinated oils make them attractive materials to use for such applications. These FC oils are characterized by very strong intramolecular interactions, yet very weak intermolecular (van der Waals) interactions [83]. This gives rise to the incredibly low surface tensions they display, in comparison to their hydrocarbon counterparts. The position of Fluorine in the upper right corner of the Periodic Chart is also responsible for the special properties found in FC oils such as their low refractive indices, viscosities similar to that of water, high fluidic densities and exceptional chemical inertness. FC oils are also considerably hydrophobic (and lipophobic) leaving them highly insoluble in water or other aqueous media, and also immiscible with hydrocarbons. To then be used in many applications, for example tar-

geting AOCs [83] or for droplet force transducers [44], these FCs should be emulsified, due to their immiscibility in both aqueous and hydrocarbon fluids.

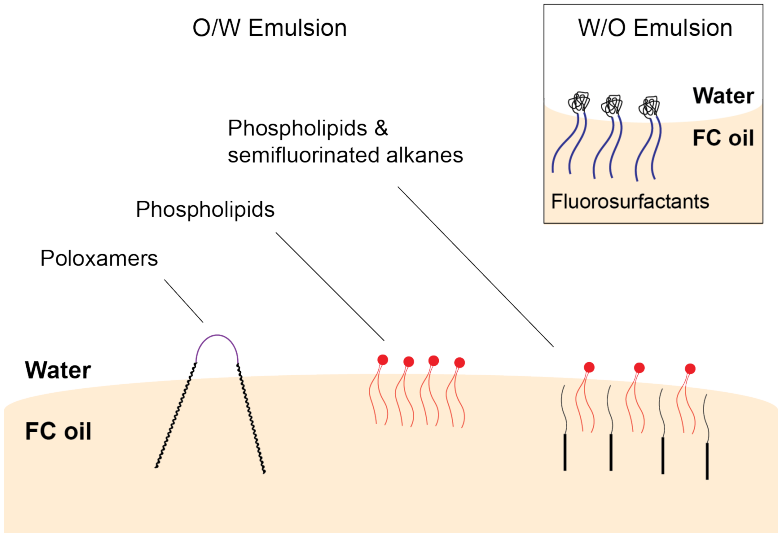

Figure 4.1: Schematic of surfactants used to stabilize emulsions utilizing FC oils. Typical surfactants to stabilize FC oil-in-water emulsions include poloxamers, and phospholipids, either alone or with semifluorinated alkanes as co-surfactants. The inset shows a schematic of a popularly-used triblock fluorosurfactant as the emulsifier in the inverse water-in-FC oil emulsion.

Stabilizing FC oil-in-water emulsions is not a trivial task, in particular due to the lack of surface active reagents (surfactants) which could stabilize them. The majority of the literature covering the stabilization of FC oil-in-water emulsions is dominated by their intended use as AOCs. Thus, a brief summary of work done to progress this research is covered. The goals for any surfactant used in emulsions used as AOCs are to lower the interfacial tension to improve dispersion of the FC oil phase into the aqueous water phase, and to stabilize the emulsion against coalescence and the diffu-

sive Ostwald ripening process (where material from smaller droplets of the dispersed phase diffuses, through the carrier phase, into droplets of larger volumes). Additionally, emulsions should not be retained within the organism for extended periods of time (hours, as opposed to days) and be excreted properly. Initial emulsions used as AOCs were stabilized with poloxamers, neutral triblock copolymers with a polyoxypropylene center, flanked by two polyoxyethylene chains (Figure 4.1). However, there were difficulties (using poloxamers as emulsifiers) in obtaining a balance between emulsions which would both be stabilized and also have an acceptable time to be retained within the organism [88]. Fluosol-DA was the first emulsion that was commercially-available as an AOC [89], and utilized a mixture of poloxamers and egg-yolk phospholipids (EYP). This emulsion system was troubled by the sensitive storage conditions and poor emulsion stability, as were most other emulsions based on Fluosol-DA [83]. From their use in the Fluosol-DA emulsion, EYPs soon became a popular component to use as the surfactant in FC oil-in-water emulsions (Figure 4.1), recognized for their improved emulsion stability compared to poloxamers [90]. Emulsions utilizing phospholipids with FCs especially in combination with perfluorooctyl bromide (PFOB), a fluorinated solvent additive chosen for its slight lipophilicity (due to the Bromine atom) and decreased water-solubility when introduced into the bulk FC oil, were particularly stable and offered more acceptable excretion rates [83]. The slight lipophilicity of PFOB better stabilizes phospholipid-based surfactants at the FC-

water interface, and these emulsions offered low interfacial tensions [83], which was thought to result in their slower Ostwald ripening rates. An additional method to further stabilize phosopholipid surfactants at the FC-water interface was through the use of semifluorinated alkanes (SFAs) - a diblock surfactant soluble in the oil phase, containing both a hydrocarbon moiety and fluorocarbon moiety (Figure 4.1). SFAs have very unique properties [91], and provide both low interfacial tension and increased stabilization of FC oil-in-water emulsions when used as co-surfactants along with EYPs [92]. However, phospholipids are sensitive materials susceptible to oxidation and hydrolysis when used in these emulsions. While the addition of co-surfactants such as SFAs can help to stabilize phospholipids at the FC-water interface, production of SFAs is difficult and still requires special storage conditions. On the other hand, using EYPs as the emulsifier in the absence of SFAs is non-ideal, due to the lipophobic nature of FCs.

Other commercially available fluorinated surfactants (fluorosurfactants) exist and can be used with FC oils. However, they are produced to stabilize the inverse water-in-oil emulsions (see inset of Figure 4.1), with a surfactant geometry which contains larger fluorinated tails compared to their smaller hydrophilic head groups. Typically, a biocompatible surfactant is synthesized from a perfluoropolyether (PFPE) starting material, containing a carboxylic acid end group, commercially named Krytox (Figure 4.2). This fluorosurfactant is usually linked to polyethylene(glycol) (PEG), to generate

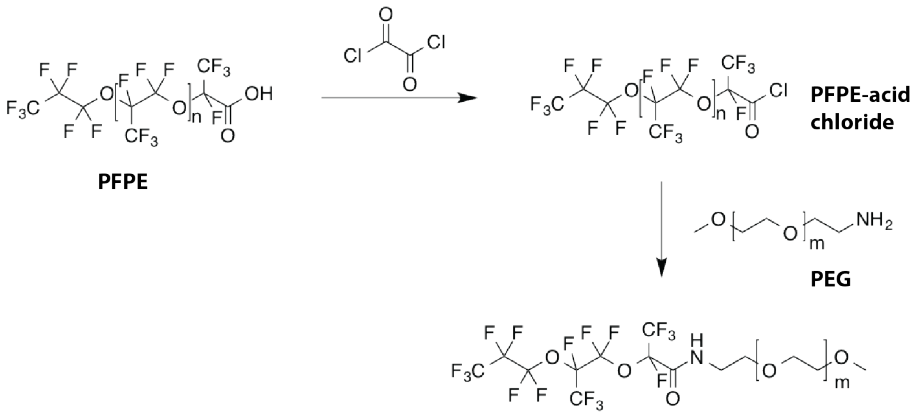

Figure 4.2: Synthetic scheme of PFPE-PEG surfactants established in the literature. PFPE-carboxylic acid is converted to PFPE-acid chloride. This is then reacted with the amine group of the PEG molecule to generate a PFPE-PEG fluorosurfactant. Unreacted starting material of the PFPE-acid chloride can become charged at FC-water interfaces, which may be problematic to use in biological studies.

a surfactant containing a the fluorinated tail group and a PEG head group [47,93] (Figure 4.2), however, others have synthesized fluorosurfactants with varying head groups and different bond types [94]. These studies demonstrate the formation of new fluorosurfacatants, however, stabilization of FC oil-in-water emulsions is not achieved (also only short-term stability is shown) and often sufficient characterization of the synthesized surfactants is not provided. Additionally, the coupling reaction between Krytox and PEG is challenging, and requires specialized solvents, making full conversion of the starting material to product difficult. As a consequence, one can expect to have leftover (unreacted) starting material. This may lead to unwanted interactions with biomolecules (e.g. proteins) when used in biological applications, and also a change

in the interfacial tension in the presence of non-ionic versus ionic media. A study showed that the interfacial tension of interfaces containing only these starting materials (polar PFPE surfactants; Krytox-FSH) will cause a substantial decrease in the interfacial tension (from its value in deionized water) in the presence of phosphate buffered saline (PBS) [48], which is used in cell culture media, for example.

Given that the literature is dominated by the use of non-ideal phospholipid surfactants or fluorosurfactants generated from ionic starting materials (and used for the inverse emulsion), the goals of the research conducted in this chapter were to develop fluorosurfactants to stabilize FC oil-in-water emulsions, while maintaining controlled interfacial tension. In a collaboration with Dr. Carolin Fleischmann (The Hawker Laboratory, UCSB), we introduce fluorosurfactants which are generated via a new synthetic approach, with a non-ionic starting material, to stabilize FC oil-in-water emulsions without the need for a co-surfactant. These new FS are tunable in geometry, enabling the control over different interfacial properties, and stabilize FC oil-in-water emulsions while avoiding special storage conditions. These FS have been fully characterized, and demonstrated to control the interfacial tension within different media while maintaining excellent control over the droplet size distribution in monodisperse emulsions generated via droplet microfluidics.

4.2 Methods

Synthesis of Fluorosurfactants

The new synthetic approach[1] is a two step reaction to couple Krytox, functionalized with a methyl ester end group (Chemours, PFPE ME), and mPEG, functionalized with a N-hydroxysuccinimide ester (NHS ester) end group (Figure 4.3). First, the ME end group on the Krytox starting material was converted to an amine (NH_2). This molecule was then reacted with the mPEG-NHS ester to create the final product. The final diblock products containing Krytox and PEG (Figure 4.3) will be referred to as Kry-PEG for the remainder of this chapter.

Synthesis of Krytox NH_2. First, 0.5 mL of methanol, 0.5 mL of Novec 7300 oil, 19 μL of ethylenediamine, and a magnetic stir bar were added to a 20 mL glass vial (Vial A). The mixture is placed on a magnetic stir plate and allowed to stir for 15 min at room temperature. During this time, 500 mg of Krytox-methyl ester was added to a separate 20 mL glass vial (Vial B), and 1.5 mL of Novec 7300 was added. This solution was vortexed for approximately 30 sec and then sonicated for 1 min, to ensure that the Krytox methyl ester was completely dissolved. The contents of Vial B were then added to reaction in Vial A by a plastic syringe, and the cap of Vial A was sealed tight.

[1] This work was done in collaboration with Dr. Carolin Fleischmann from The Hawker Lab, UCSB.

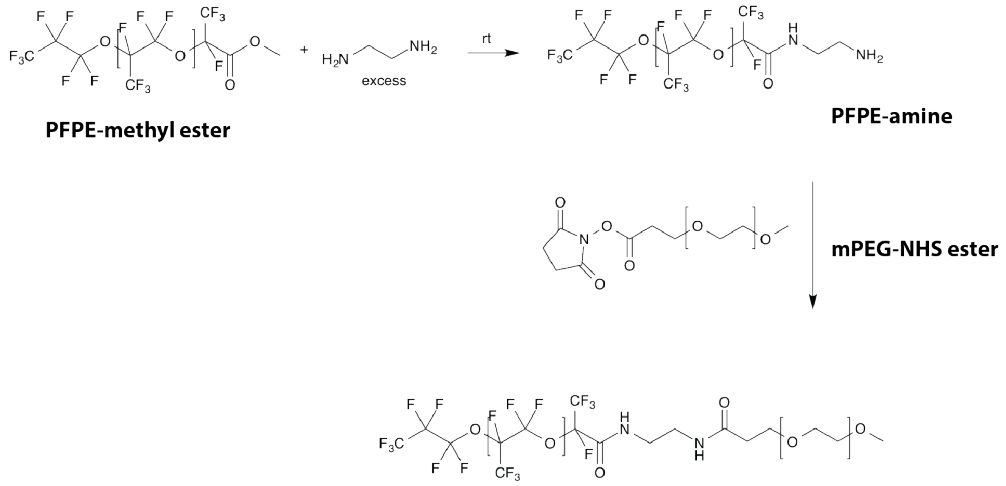

Figure 4.3: New synthetic scheme of PFPE-PEG surfactants. PFPE-methyl ester is converted to PFPE-amine. This is then reacted with mPEG-NHS ester to generate diblocks of the final PFPE-PEG product (Kry-PEG) from non-ionic starting materials.

This reaction was then allowed to proceed under constant stirring for two days at room temperature.

After two days, the reaction mixture was transferred to a 15 mL centrifuge tube via a glass pipette. Vial A was rinsed with additional Novec 7300, and this mixture was also transferred to the centrifuge tube, to recover any leftover materials. All excess solvents were then removed. The leftover viscous residue was then dispersed in dichloromethane (DCM) in a 15 mL falcon tube, via short cycles of vortex mixing and sonication. Aterwards, the mixture was centrifuged for 10 min. The supernatant (mostly DCM) was removed and discarded via pipette and the residue was redispersed in fresh DCM. Once again, the mixture was dispersed in DCM via short cycles of vor-

tex mixing and sonication, prior to centrifugation for another 10 min. Overall, this process was repeated until the mixture had been redispersed in DCM and centrifuged for a total of three cycles. The residue was then dissolved in approximately 2 mL of Novec 7300 oil and transferred to a glass vial (with the weight of the vial+cap noted). The volatile Novec 7300 solvent was then removed by applying a constant air stream over the open glass vial for 1 hr. The remaining viscous oil was then dried in a vacuum oven over several hours, at 50 $^{\circ}C$. The remaining material can be characterized via infrared (IR) spectroscopy to verify that the desired Krytox-NH_2 was indeed formed - the introduction of the amide group is characterized by a shift in the wavenumber, corresponding to the amide absorption band (Figure 4.4).

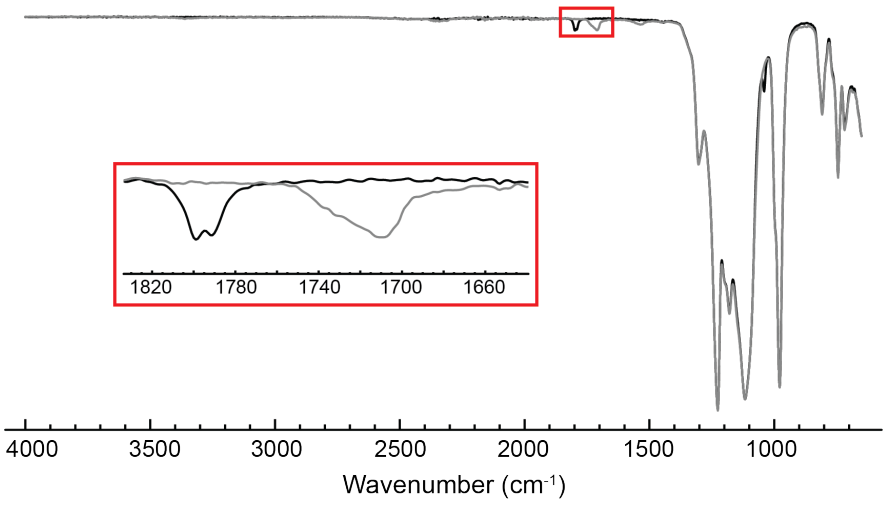

Figure 4.4: IR characterization of first reaction step. IR spectra of Krytox-methyl ester (black), and Krytox-NH_2 (gray). Introduction of the amide group is demonstrated through a shift in the wavenumber, corresponding to the amide absorption band (inset).

Coupling of Krytox NH_2 and mPEG-NHS ester to form Kry-PEG Fluorosurfactants. Inside a 20 mL glass vial with a septa-screw cap (containing a magnetic stir bar), the mPEG-NHS ester material was added based on the molecular weight (MW) of the PEG group to be used in the synthesis:

- MW 1000 Da: 72 mg
- MW 550 Da: 40 mg
- MW 350 Da: 25 mg

This reaction vial was then purged, through the septum, with argon for 10 min, to prevent any moisture from being present during the reaction. In the meantime, a heating block was preheated to 50 $^{\circ}C$. The temperature was monitored with a thermometer, and allowed to equilibrate for at least 5 min. Afterwards, 0.5 mL of trifluorotoluene (TFT) was added to the mPEG-NHS ester vial via syringe and needle. Parafilm was then wrapped around the septa cap, to isolate the reaction. This mixture was then vortexed and sonicated to encourage dispersion of the mPEG-NHS ester into the TFT. Based on the MW of the PEG group, this required different mixing times - higher MW PEG will be more difficult to dissolve in the fluorinated TFT solvent, and thus requires more mixing time. In a separate glass vial, 150 mg of the Krytox-NH_2 was dissolved in 0.5 mL of Novec 7300 oil via brief vortexing and sonication. This solution was then slowly dispensed via syringe and needle, through the septum of the reaction vial. Af-

terwards, the parafilm of the reaction vial was replaced (due to the hole just created by addition of the Krytox-NH_2 product) and allowed to stir on a magnetic stir plate for 10 min at room temperature. Finally, the reaction is transferred to the pre-warmed heating block at 50 $^{\circ}C$, and stirred for 3 days at this elevated temperature. The work up procedure of the reaction was done as previously mentioned for the Krytox-NH_2 material. Briefly, the reaction mixture was transferred to a 15 mL falcon tube, where the solvents were then removed by a constant air stream applied for at least 1 hr. The mixture is them dispersed in DCM and centrifuged for at least 3 cycles, as mentioned above, in **Synthesis of Krytox NH_2**. Finally, the residue was dissolved in Novec 7300 and transferred into a glass vial (with the weight noted). All solvents were then removed by a constant air stream, after which the product was placed into a vacuum oven for several hours (typically overnight) at 50 $^{\circ}C$.

IR Spectroscopy of Fluorosurfactants

IR spectroscopy was used to identify characteristic functional groups for both starting materials and final products. An IR spectrometer was used along with Spectrum 10 software to analyze and export spectra of all materials. The instrument was initialized, and the background (to be subtracted off the sample signal) was determined by scanning an empty sample window first, which was wiped clean with acetone and a Kimwipe. Then, a small amount (several milligrams) of the desired sample was placed

onto the stage using a glass pastuer pipette and the sample window was scanned again to obtain the IR spectrum.

Interfacial Properties of Fluorosurfactants

To characterize the interfacial tension of the droplets prepared with the newly synthesized KryPEG fluorosurfactant, similar protocols were followed according to the Methods section of Chapter 2. Accordingly, an optical tensiometer (Biolin Scientific, Theta Optical Tensiometer) was used to measure equilibrium interfacial tension values. Fluorocarbon oil droplets (either neat or containing surfactants) were suspended from syringe needles (typically 25 gauge, Jensen Global, JG25-1.0X 50) while immersed within an aqueous media inside of a cuvette (BRAND, 759170). Automated software from the tensiometer enabled detection of the interface and calculated (using the Young-Laplace equation) the resulting interfacial tension between the two fluids. Three measurements were taken over several minutes to 0.5 hours, depending on the surfactant concentration used, for all combinations of oil and surfactants to enable average measurements of equilibrium interfacial tension values.

Temporal Emulsion Stability

To test emulsion stability, both bulk emulsification was used (testing short-term stability) and emulsification via microfluidics was utilized (for testing long-term sta-

bility), as previously described in the Methods section of Chapter 2. Accordingly, bulk emulsions were generated by hand [46] (Figure 2.3). A 4 mL glass vial was coated with a 0.1% (w/w) BSA solution, rinsed with deionized water and then 1 mL of deionized water was added, in lieu of adding the DSPE-PEG(2000)-biotin surfactant which was previously required to stabilize FC oil-in-water emulsions. Approximately 100 μL of fluorocarbon oil (containing the desired KryPEG fluorosurfactant) was added to the vial. The vial was then vigorously shaken by hand (Figure 2.3A) to generate a course emulsion. Afterwards, a pipettor with a 1 mL tip was used to rapidly aspirate and dispense the oil against the glass vial (generating large shear stresses) to narrow the size distribution of the resulting polydisperse emulsion (Figure 2.3B). Short-term stability of the resulting emulsion was checked by imaging on an inverted microscope over several minutes.

To make monodisperse emulsions, we utilized the same 20 μm glass microfluidic devices used in the Methods section of Chapter 2. Accordingly, to ensure that the surfaces were sufficiently hydrophilic and to prevent wetting of the droplet phase, the channel walls were coated with a 1% (w/w) solution of bovine serum albumin (BSA). To this end, BSA was flowed through the channels for 30 minutes, followed by a rinse with deionized water (purified through a Milli-Q purification system) by flowing water through the channels for at least 30 minutes, prior to generating droplets. Droplets were generated with a continuous (outer) phase (CP) of deionized water, without the

addition of the DSPE-PEG(2000)-biotin (Avanti Polar Lipids, 880129) previously required to stabilize the FC oil-in-water emulsions. The disperse (inner) phase (DP) consisted of 2% (w/w) of the desired KryPEG fluorosurfactant dissolved in Novec 7300 oil (3M, 98021248285). Droplet collection and microfluidic device cleaning followed the same procedures as described in the Methods section of Chapter 2.

4.3 Results and Discussion

Characterization of Kry-PEG Fluorosurfactants

Several techniques were used to characterize the Kry-PEG fluorosurfactant products including IR spectroscopy, nuclear magnetic resonance (NMR) spectroscopy, and mass spectrometry (MS). I performed experiments to obtain IR spectra while the remaining characterization data was obtained by Dr. Fleischmann (The Hawker Laboratory, UCSB), and was interpreted to further support fluorosurfactant formation[2].

IR spectroscopy supports fluorosurfactant formation by the observation of certain functional groups when comparing the starting materials to the final products (Figure 4.4 and Figure 4.5). Observing Figure 4.4, the methyl ester functional group (with an absorbance band at approximately 1795 cm^{-1}) is no longer present in the

[2]The collaborating group further characterized Kry-PEG fluorosurfactants via ^{1}H NMR, ^{19}F NMR, ^{1}H Diffusion Ordered SpectroscopY (DOSY) NMR and matrix-assisted laser desorption/ionization (MALDI) mass spectrometry.

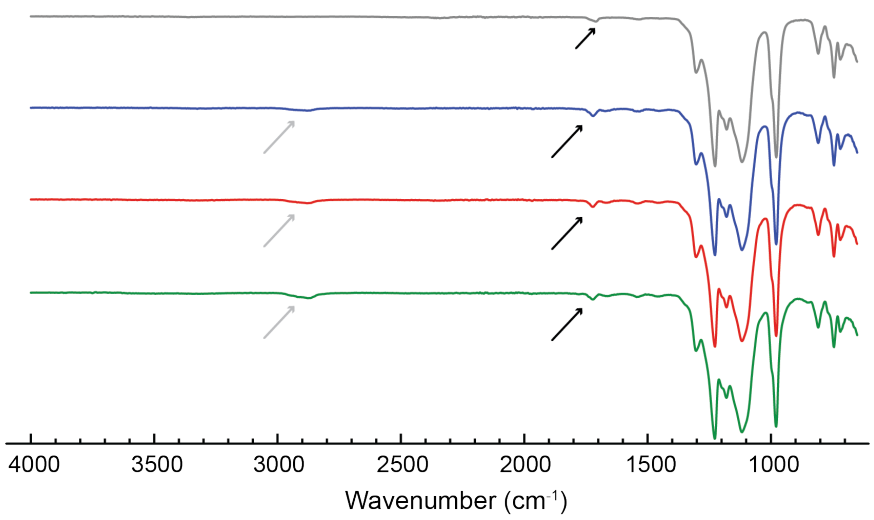

Figure 4.5: IR characterization of fluorosurfactants. IR spectra of Krytox-NH_2 (gray), Kry-PEG(350) (blue), Kry-PEG(550) (red), and Kry-PEG(1000) (green). All Kry-PEG fluorosurfactants show a similar absorption band at 1720 cm^{-1} for the amide group (black arrows) that the Krytox-NH_2 contains at 1710 cm^{-1}. Additionally, the Kry-PEG fluorosurfactants show an absorption band indicating the presence of the PEG block (gray arrows).

Krytox-NH_2 material. Instead, the absorbance band is shifted to 1710 cm^{-1}, due to the presence of the amide bond in the Krytox-NH_2 material. All fluorosurfactants, namely Kry-PEG(350), Kry-PEG(550) and Kry-PEG(1000), were also characterized by IR spectroscopy (Figure 4.5). Each fluorosurfactant shows an absorbance band at $\sim$2900 cm^{-1}, corresponding to the PEG block, which is absent in the Krytox-NH_2 starting material (Figure 4.5, gray arrows). Furthermore, the absorbance band of the amide group is present at 1720 cm^{-1} in all fluorosurfactant products, shifted slightly from the band of the Krytox-NH_2 starting material, likely attributed to the incorporation of a second amide group in the final product (Figure 4.3, black arrows). Taken together, along

with all NMR and MALDI/MS characterizations, IR spectroscopy strongly supports the formation of all three fluorosurfactants.

Kry-PEG Fluorosurfactants: Interfacial Properties

Important to a surfactant's characteristics are its effectiveness and efficiency in modifying the interfacial tension of a particular system. A highly efficient surfactant will produce a given change in surface or interfacial tension at lower concentrations, while a highly effective surfactant will provide, overall, a larger reduction in interfacial tension, regardless of the concentration [95]. Generally, a surfactant's efficiency is the concentration of surfactant needed to provide a reduction of surface (or interfacial) tension of 20 mN/m, indicating the minimum concentration required to produce the maximum surfactant adsorption. To determine these characteristics of the synthesized FS, we measured the interfacial tension of KryPEG(350), KryPEG(550) and KryPEG(1000) as a function of FS concentration in deionized water (Figure 4.6). We observed that the FS with smaller PEG head groups (KryPEG(350) and KryPEG(550)) are more effective, achieving a lower maximum reduction in interfacial tension than the FS containing the largest head group. Interestingly both of these FS reach similar interfacial tension values at their maximal reduction, around 5-6 mN/m (Table 4.1). It is apparent that KryPEG(550) is the most efficient of the three FS investigated, as KryPEG(550) reaches a reduction in interfacial tension by 20 mN/m (from $\sim$35-15

mN/m) at a concentration that is one order of magnitude smaller than the concentrations required of KryPEG(350) and KryPEG(1000) (Figure 4.6). From Figure 4.6, it is also evident that KryPEG(1000) is the least effective surfactant, providing an overall maximum reduction in interfacial tension of ∼20 mN/m.

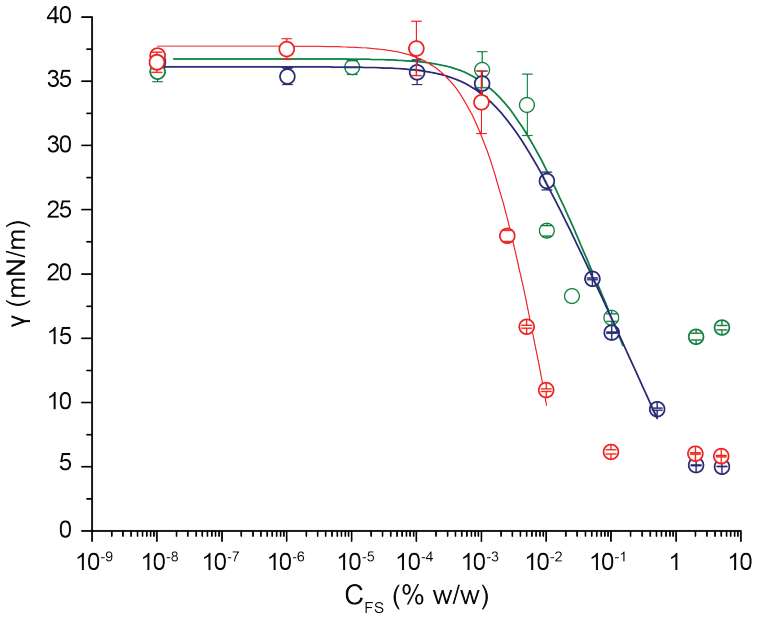

Figure 4.6: Fluorosurfactant efficiency and effectiveness. Equilibrium interfacial tension versus fluorosurfactant concentration (C_{FS}) for KryPEG(350) (blue), KryPEG(550) (red), and KryPEG(1000) (green). The Gibbs adsorption equation was used to fit data in the dilute surfactant regime.

Surfactant	γ_{min} (mN/m)	Γ_∞ (μmol/m^2)	a (nm^2)
KryPEG(350)	5.1	1.99	8.35
KryPEG(550)	5.9	5.58	2.98
KryPEG(1000)	15.5	2.17	7.67

Table 4.1: Properties of fluorosurfactants.

To investigate the surfactant packing at the FC oil-water interface, the saturating suface excess concentration (Γ_∞) was obtained by fitting the data (in the dilute regime) using the Gibbs adsorption equation [48], as done in Chapter 2 (Equation 2.2). Surface excess concentrations for KryPEG(350), KryPEG(550) and KryPEG(1000) were determined to be Γ_∞ = 1.99, 5.58, and 2.17 μmol/m^2, respectively (Table 4.1). Knowing Γ_∞ enables the area occupied per surfactant molecule at the interface (a) to be determined, via:

$$\text{Area}\,[\text{nm}^2] = a = \frac{10^{18}}{\Gamma_\infty N_A} \tag{4.1}$$

where N_A is Avagadro's constant. The area per surfactant molecule at the FC-water interface for KryPEG(350), KryPEG(550) and KryPEG(1000) was determined to be 8.35, 2.98 and 7.67 nm^2, respectively (Table 4.1). Due to having the smallest interfacial area, it is suspected that KryPEG(550) packs more tightly at the interface. This is supported further by the fact that not only does KryPEG(1000) have a larger area, but KryPEG(350) does as well. KryPEG(1000) may pack less tightly at the interface due to the larger PEG head group, ultimately limiting the amount of surfactant molecules that can pack per given area. Interestingly, KryPEG(350) has an area similar to that of KryPEG(1000). This indicates that the surfactant is likely not oriented vertically, but rather assuming some random or more horizontal orientation, which would also limit the number of surfactants able to pack per given area.

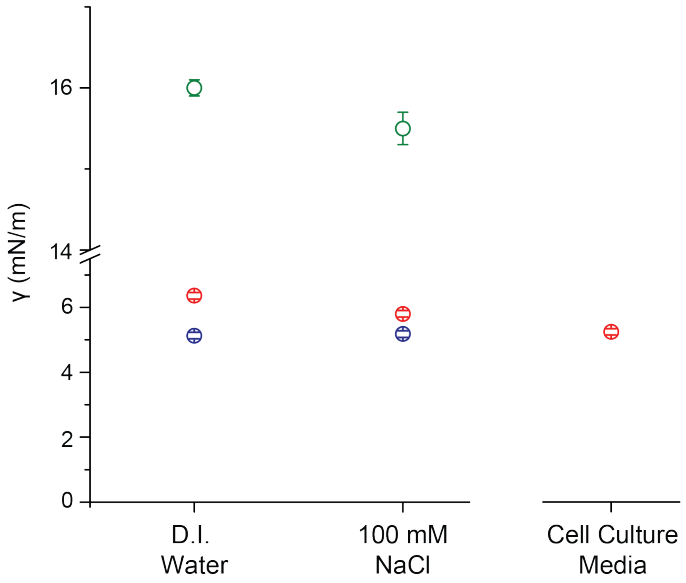

Figure 4.7: Behavior of fluorosurfactant in presence of high concentrations of salt and small surface active molecules. Equilibrium interfacial tension measurements were performed with Novec 7300 containing 2% w/w of each fluorosurfactant KryPEG(350) (blue), KryPEG(550) (red) and KryPEG(1000) (green). Measurements were done in D.I. water, 100 mM NaCl, and cell culture media (containing 10% fetal bovine serum).

We further investigated the fluorosurfactant behavior in the presence of high salt concentrations and small surface active molecules (Figure 4.7. Each of the fluorosurfactants (used at 2% w/w in Novec 7300) showed less than a 10% decrease in interfacial tension, from values measured in D.I. water, in the presence of 100 mM NaCl. Specifically, the interfacial tension values decreased by 1.0%, 8.8% and 3.1% for KryPEG(350), KryPEG(550) and KryPEG(1000), respectively. This demonstrates that the synthesized fluorosurfactants are non-ionic, and preventing changes in interfacial tension in the presence of high salt concentrations. Finally, the interfacial

tension using KryPEG(550) was measured in cell culture media, which is a complex chemical environment containing high salt concentrations and many small surface active molecules. From the data represented in Figure 4.7 we found that the interfacial tension decreases by approximately 17.5%, an improvement over the commercially-available, non-ionic triblock fluorosurfactant (which decreased by ∼25%) [96]. Thus, using the fluorosurfactant at high concentrations, KryPEG(550) alone is able to shield the interface and prevent undesired changes in interfacial tension in the presence of a variety of small molecules and high salt concentrations.

Kry-PEG Fluorosurfactants: Emulsion Stabilization

A primary purpose of any surfactant used as an emulsifier is to stabilize the emulsion against coalescence, as well as other methods of emulsion destabilization [97]. An ideal surfactant would stabilize a monodisperse emulsion indefinitely, however, in practice this is not achieved and the change in emulsion size distribution should be monitored over time. Here, bulk emulsification was initially used to generate polydispserse FC oil-in-water emulsions, to quickly rule out surfactants which could not immediately stabilize an emulsion over several minutes. In this case, Kry-PEG(1000) and Kry-PEG(550) stabilized polydisperse emulsions while Kry-PEG(350) did not (data not shown). To assess how well the synthesized fluorosurfactants stabilized an emulsion over longer periods of time, microfluidics was used to generate monodisperse FC

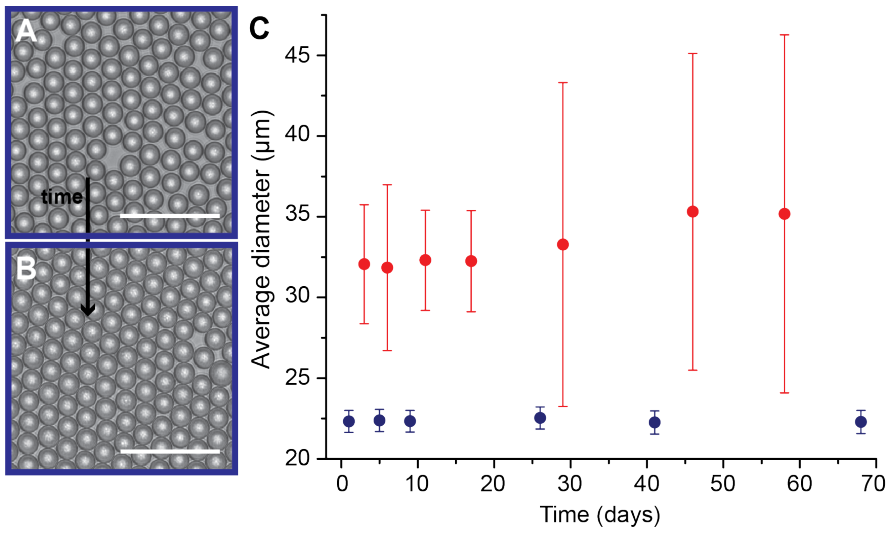

Figure 4.8: Kry-PEG fluorosurfactants stabilize FC oil-in-water emulsions. A monodisperse emulsion of Novec 7300 oil with 2% (w/w) of Kry-PEG(550) 1 day after generation (A) and 90 days after generation (B) with microfluidics. (C) Average droplet size during long-term storage at room temperature for emulsions stabilized with Kry-PEG(550) (blue) and KrytoxPEG(600)+DSPE-PEG(2000)-biotin (red).

oil-in-water emulsions. Given that KryPEG(550) was the most efficient surfactant with the closest interfacial packing, these surfactants were investigated for long-term emulsion stability. Using commercially-available, glass microfluidic devices we generated monodisperse, stable FC oil-in-water emulsions using Novec 7300 as the dispersed (droplet) phase in the absence of other surfactants. We observed that Kry-PEG(550) stabilized FC oil-in-water emulsions exceptionally well, maintaining a seemingly constant average droplet size over several months (Figure 4.8C). For comparison, the average droplet size of an emulsion stabilized using both commercial Krytox-PEG(600) and DSPE-PEG(2000)-biotin was also measured over time. While the two-surfactant

system provides emulsion stability initially, the average droplet size increases starting around 30 days. The increase in size around this time may coincide with the degradation, likely due to hydrolysis, of the phospholipid-based surfactant which is what stabilizes the emulsion. It can also be observed from Figure 4.8 that the standard deviation of the droplet size also increases over time, indicating that the emulsion is coarsening.

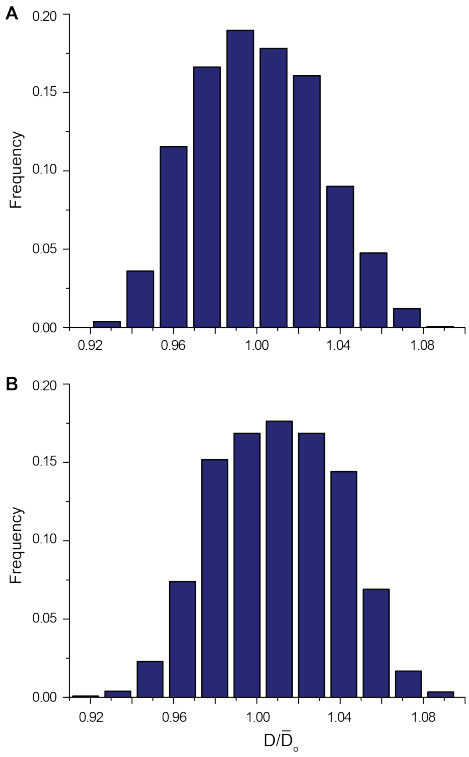

Figure 4.9: Droplet size distribution of an emulsion stabilized with KryPEG(550). A monodisperse emulsion was generated using Novec 7300 containing 2% (w/w) KryPEG(550) using microfluidic devices. The droplet size was measured over time at day 0 (A) and again at day 26 (B). At least N = 1000 data points were used to study the droplet size distribution of the emulsion. All droplet size measurements were normalized to the initial average droplet diameter $\bar{D}_o$.

Additionally, the droplet size distributions of the emulsion stabilized with KryPEG(550) and Krytox-PEG(600) + DSPE-PEG(2000)-biotin were also investigated over time. Over approximately 30 days, there is a clear difference in the stabilization between these two emulsions: Figure 4.9 shows that the new KryPEG(550) fluorosur-

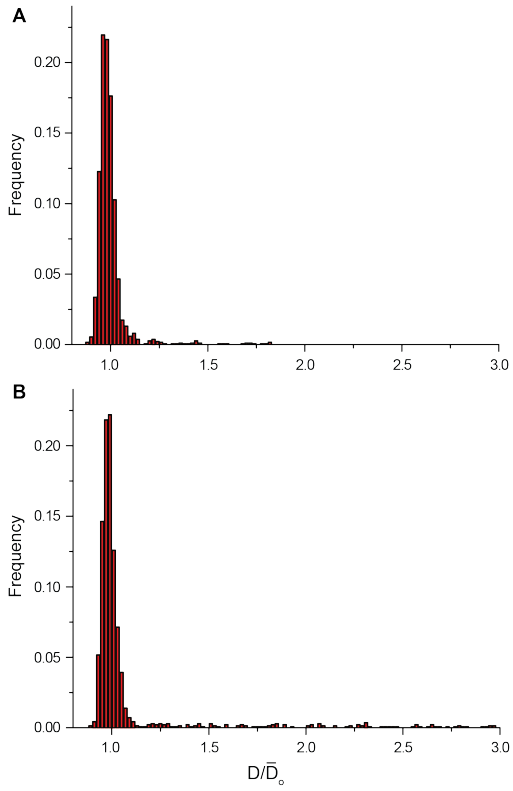

Figure 4.10: Droplet size distribution of an emulsion stabilized with Krytox-PEG(600) and DSPE-PEG(2000)-biotin. A monodisperse emulsion was generated using Novec 7300 containing 2% (w/w) Krytox-PEG(600) (coated with DSPE-PEG(2000)-biotin) using microfluidic devices. The droplet size was measured over time at day 3 (A) and again at day 32 (B). At least N = 1000 data points were used to study the droplet size distribution of the emulsion. All droplet size measurements were normalized to the initial average droplet diameter $\bar{D}_o$.

factant stabilizes the emulsion well, because the droplet size distribution (normalized by the initial average droplet diameter $\bar{D}_o$) remains largely time-independent. On the other hand, the distribution of droplet sizes using the two-surfactant system shows a population of droplets centered around the starting (targeted) droplet size, with several additional peaks at $D/\bar{D}_o$ greater than 1, indicating a coarsening of the emulsion (Figure 4.10). This coarsening over time is likely due to a mainly coalescence-driven destabilization of the emulsion. Consider two droplets A and B, which are the same size (of equal volume $V_A = V_B$) which coalesce into a larger droplet C. Mass conser-

vation dictates that

$$V_C = V_A + V_B \tag{4.2}$$

Rewriting with $V_A = V_B = \frac{4}{3}\pi(\frac{D}{2})^3$, where D is the initial droplet diameter (of droplets A and B), yields:

$$\frac{4}{3}\pi(\frac{D_C}{2})^3 = \frac{4}{3}\pi(\frac{D}{2})^3 + \frac{4}{3}\pi(\frac{D}{2})^3 \tag{4.3}$$

Simplifying this we find that the size of droplet C is $D_C = D\sqrt[3]{2}$. This can be generalized for the coalescence of $N = 2, 3, 4...$ droplets as $D_C = D\sqrt[3]{N}$ for likely cases where, for example, two previously coalesced droplets merge with a third droplet ($N = 3$). Indeed, we observe from Figure 4.10 that additional peaks at D/$\bar{D}_o$ greater than 1 correspond to values which are indicative of coalescence of the droplets.

Previous studies have investigated emulsion stability of FC oil-in-water emulsions using different combinations of phospholipids, semifluorinated alkanes (SFAs) and oil additives [92]. While good stabilization of the emulsion is achieved using phospholipid and SFAs as co-surfactants (to stabilize the phospholipids at the FC-water interface), this requires custom synthesis and specialized storage conditions, as phosphilipids temperature sensitive and prone to hydrolysis at the interface [83]. Here, we utilize commercially available reagents in a two-step synthesis to produce fluorosurfactants

that provide long-term stability of FC oil-in-water emulsions at room temperature, by only using a single surfactant.

4.4 Conclusion

In this chapter, we present novel synthesis and characterization of fluorosurfactants. In contrast to previously established methods, these fluorosurfactants are generated from completely non-ionic starting materials, enabling their use in biological applications which may contain molecules (e.g proteins) susceptible to influence by charged surfactants. The new fluorosurfactants offer superb stabilization of fluorocarbon oil-in-water emulsions, without the need for an additional co-surfactant. Additionally, the products were well characterized using several characterization methods, to ensure formation of the desired fluorosurfactants. The ability of the flourosurfactants to provide long-term emulsion stabilization makes them potential candidates to be used as the emulsifier in artificial oxygen carriers.

Chapter 5

Concluding Remarks and Future Directions

The measurement of mechanical forces in biological systems is not an easy task, especially concerning 3D measurements done *in situ*, for both systems *in vitro* and *in vivo*. The introduction of oil droplets to be used as force transducers [44] provided the biophysics community with a method to conduct such studies, under these demanding experimental conditions. However, as described in Chapter 2, limited control over the different properties of the droplets, along with the use of custom-made surfactants, impeded the practical use of the method in a variety of systems to measure cell-generated stresses. The goals of the research conducted throughout Chapters 2-4 were to address these issues, and to utilize this tool to investigate internal stresses

within growing, 3D tissues. This is summarized below, in addition to future work proposed for each project:

Microdroplets to Measure Cell-generated Mechanical Stresses

The proof-of-principle method utilizing droplets as force transducers was a pioneering work which addressed an important gap in biophysical methods: a lack of tools available to measure local 3D forces in biological systems *in vivo* (and *in vitro*). However, the method did contain its limitations, which were addressed in the optimization of this method. The goals of the research conducted in Chapter 2 were to control the interfacial tension and droplet size, while developing a reliable approach to ensure that accurate cell-generated stresses could be measured both *in vitro* and *in vivo*.

The new, two-surfactant coatings of the droplets and the use of microfluidics for droplet generations allow full control over the relevant parameters. While other studies typically use the fluorocarbon oil as the continuous phase for various experiments [47, 48, 52] (for water-in-oil emulsions), we were able to develop a reliable approach using only commercially-available microfluidic components to generate highly monodisperse fluorocarbon oil-in-water emulsions. Full control over droplet size, in addition to proper shielding of the interface in complex chemical environments, allow these new droplet sensors to be used in a variety of systems as force transducers, ei-

ther *in vitro* or in *in vivo*. Altogether, this work has made the production of droplets to be used as force transducers accessible to the scientific community, utilizing materials and equipment available in most laboratories.

While the current two-surfactant system stabilizes the droplets, it should be noted that the fluorourfactant alone does not stabilize fluorocarbon oil-in-water (O/W) emulsions. Problems may arise from the use of a nonideal (hydrocarbon) surfactant such as the DSPE-PEG(2000)-biotin, particularly given that a phosphilpid surfactant is used to mediate the interactions between cells and droplets (due to its functionalization with the biotin group). For the DSPE-PEG(2000)-biotin surfactant used, hydrolysis may occur (removing the streptavidin and ligand molecules) which would compromise both the fluorescence of the droplet, and also the adhesive interactions between neighboring cells and the droplet. Additionally, due to the inability of the Krytox-PEG(600) fluorosurfactant to stabilize FC oil-in-water emulsions alone, degradation of the DSPE-PEG(2000)-biotin may also compromise the emulsion stability. The lack of suitable, commercially-available fluorosurfactants leaves few options to stabilize these O/W emulsions in general, and fewer to stabilize these droplets to be used as force transducers, with phospholipid-based surfactants being the typical solution [83, 90]. While these phospholipid systems work, especially in combination with co-surfactants [92, 98], the preparation and storage of such an emulsion is nontrivial. Thus, we sought to improve the long-term stabilization of fluorocarbon O/W emulsions through use

of a custom-made fluorosurfactant. Through a simple two-step synthesis, surfactants produced to stabilize these emulsions have been created, to further improve the microdroplet-based method (discussed in Chapter 4).

It should be noted, as described in [44], that this technique does not allow the measurement of isotropic nor shear stresses. Using this method, local normal stresses which are applied non-homogeneously (e.g. anisotropically) to the droplet surface, can be quantified. Isotropic stress would apply a homogeneous surface stress to the droplet. Due to the incompressibility of the oil droplet, this uniform stress would not induce a deformation on the droplet surface. In cases where it is desired to measure both anisotropic and isotropic stresses, the droplet technique can be combined with elastic microbeads, which were recently used to measure isotropic stresses within tumor spheroids [43]. This combination can provide insight into the stresses that cells are experiencing *in situ*, which arise from both uniform stresses and differences in cell-cell stresses.

Measurement of Spatiotemporal Cell-generated Stresses within 3D Spheroids

By investigating mechanical stresses within multicellular spheroids, widely used as model 3D tissues and tumors, we can help understand how mechanics influence cell behavior in 3D multicellular environments. The use of novel tools such as droplet-

based probes or elastic microbeads can complement cell and molecular biological studies to provide an insight on how physical quantities correspond with molecular cues in 3D multicellular environment. We were able to investigate normal stresses within model 3D tissues, and demonstrate that differences in these cell-generated (cell-scale) stresses are not established within 3D cell aggregates spatially, however, the magnitude increases over time. While these stresses were endogenous in nature (e.g. measuring the growth-induced stress), stresses due to external compression may also be investigated. Along with using a cancerous cell-line, these experimental conditions create physiologically relevant models of solid tumors, a future direction which is further discussed below.

One proposed extension to this research is to use the new oil droplets as force transducers within breast cancer cell spheroids. These experiments will guide the interpretation of the role of mechanics, and patterns in stress during tumor growth. Similar to the work previously discussed in this chapter, stresses can be quantified within spheroids of cancerous and non-cancerous mammary epithelial cell lines, in free suspension. There are several cell lines to choose from: a very popular, highly-malignant cell line MCF-7 forms spheroids using several methods [99, 100, 101] and is commercially available as a transgenic line expressing cytoplasmic GFP, hence enabling fluorescent imaging. A highly-used non-tumorigenic cell line is the MCF10A cell line, which has also been shown to form spheroids [102]. These cell lines will enable a

comparison between stresses generated within a non-tumorigenic (e.g. MCF10A) and a malignant (e.g. MCF-7) model tumor. Droplets can be injected at early time points ($<$24 hr) of aggregation into spheroids, which can be allowed to compact over 3-5 days. Approximately 5-10 drops can be injected and stresses, due to the pushing and pulling forces applied by surrounding cells normal to the drop surface, can be measured for the different regions established within the spheroid: the core, the quiescent middle and the proliferative rim [53]. Measurements performed in free suspension will provide data on stresses induced by growth of the tumor spheroid, and enable comparisons between stresses in a cancerous model tumor, and a non-cancerous model tumor. Here, we would expect to measure higher stress levels in cancerous model tumors compared to model tumors made of non-tumorigenic cells, as supported by [64].

It has been suggested that anisotropies in stress exist within cancerous cellular spheroids [62, 63], and that the cells within these tumor spheroids align themselves radially near the core, and tangentially around the periphery [63]. It would then be interesting to observe the droplet deformation in tumor spheroids where such arrangement might exist, in particular looking at the orientation of the droplet in regions of the core compared to those near the periphery. The reconstruction algorithm used to determine the droplet curvature [70] is capable of fitting ellipsoids to experimental droplets, enabling the quantification of the major and minor axes and its orientation.

Altogether, it is possible to investigate these potential anisotropies in stress by using the droplets in tumor spheroids.

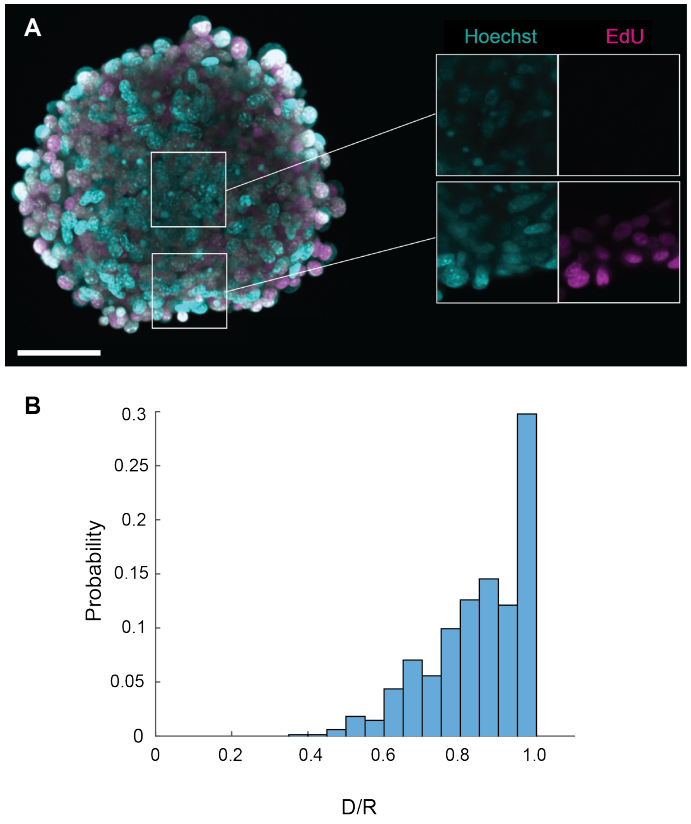

Figure 5.1: Proliferation gradient within tooth mesenchymal cell spheroids. (A) Maximum intensity projection of a 72 hour formed spheroid showing nuclei (cyan) and dividing cells (magenta) using the Click-iT EdU proliferation assay (left). Confocal sections of regions either at the periphery or close to the core (right). Scale bar 50 μm. (B) Histogram of proliferation profile within mesenchymal cell spheroid showing that dividing cells are localized closer to the periphery.

Additionally, because the influence of mechanical inputs has been shown to alter cell proliferation, density and flows within tumor spheroids [6, 63], these may also be investigated for their potential correlation with stresses developed in tumor spheroids. Using standard immunofluorescence methods, cell proliferation, viability (live/dead assay), and density may be investigated, in addition to cell flows within these tumor spheroids. Preliminary data has been obtained to measure proliferation in mesenchymal cell spheroids using 5-Ethynyl-2'-deoxyuridine (EdU), a thymidine ana-

logue, which is incorporated into DNA during active DNA synthesis (ThermoFisher Scientific, C10337). Dividing cells can be imaged using confocal fluorescence microscopy using this assay, however, care should be taken considering the aggregate size: imaging 3D tissues is more difficult using confocal microscopy when the tissue is very large (typically thicker than 100μm). The preliminary proliferation assay demonstrates the existence of a spatial gradient in proliferation within the spheroid (Figure 5.1), as previously described [6, 53]. Here, D is the droplet distance from the spheroid center, while R is the average aggregate radius.

Finally, the tumor spheroids (containing drops) can be embedded within artificial matrices, in order to better recapitulate the natural tumor microenvironment, which provides some resistance to growth. Using a mixture of Collagen1 and Matrigel in different proportions, as done in [103], can tune the stiffness of the surrounding microenvironment. Embedment within such an artificial matrix will provide resistance to spheroid growth, much like the resistance a tumor would encounter from the surrounding tissues. Thus, while spheroids in free suspension enable stresses induced *solely by tumor growth* to be studied, embedded spheroids allow the investigation of stress, influenced by resistance from the surrounding microenvironment [64]. Drops can be injected into spheroids at early time points of aggregation ($<$24 hr), and afterwards embedded within artificial matrices of varying stiffness. The same experiments will be performed as in the free suspension case to quantify surface normal stresses

and investigate cell proliferation, density, viability and cell flows, now in the case of spheroids embedded within artificial matrices. Mammary epithelial cells may invade into the surrounding matrix at high stiffness [20, 103]. This provides a potential avenue for further investigation, as invasion is an interesting phenomenon requiring highly mechanical behavior of cancer cells and the surrounding microenvironment [19, 104]. However, if it is desired to avoid invasion during the observation of tumor growth, agarose gels that are not impaired by the matrix-degrading molecules secreted by cells can be used, as done in [9]. Altogether, in combination with the newly developed droplet force transducers, these approaches can provide novel insight into stresses internal to model tumor spheroids. Spheroids in free suspension enable the investigation of stresses induced solely by growth, while embedded spheroids allow the investigation of stresses from a resistance to growth by the surrounding environment.

New Fluorosurfactants for Stabilizing Fluorocarbon Oil-in-water Emulsions

Following a new synthetic approach[1], we were able to synthesize novel, nonionic fluorosurfactants to stabilize FC oil-in-water emulsions. By investigating the interfacial properties of these new fluorosurfactants we were able to determine the optimal

[1]This work was done in collaboration with Dr. Carolin Fleischmann from The Hawker Lab, UCSB.

surfactant geometry to maximize interfacial packing and ensure long-term emulsion stabilization. While we have demonstrated that these surfactants provide control over the interfacial tension and stabilize microemulsions, future work can be done to extend their use in a variety of applications.

Targeting their use as artificial oxygen carriers [75,83,84,85], FC oil-in-water emulsions typically contain droplet diameters on the order of 100 nm. We have demonstrated the capability of our custom fluorosurfatants to stabilize microemulsions, however, future work may focus on using them to stabilize nanoemulsions. As done in Chapter 4, the nanoemulsion stability should be monitored over time, while paying attention to the average droplet size, as well as the size distribution. To best demonstrate their potential use as artificial oxygen carriers, the nanoemulsions should be subjected to relevant storage conditions. This can be achieved by checking emulsion stability at elevated temperatures, and in a media which contains small molecules and varying salt concentrations (such as cell culture media). Control experiments which may serve to investigate emulsion destabilization can be designed to store emulsions solely in salt solutions, solely at elevated temperatures, or solely in the presence of small proteins.

A previous study has investigated the stability of inverse (water-in-FC oil) emulsions either containing salts or at elevated temperatures [93]. Both the presence of salts and elevated temperatures were found to destabilize microemulsions, over

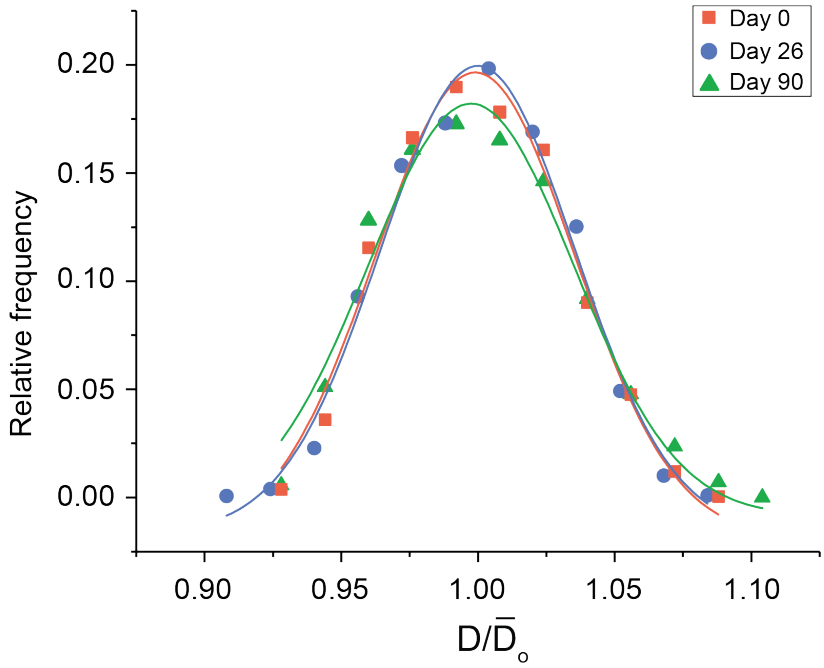

Figure 5.2: Emulsion stability over time using Kry-PEG(550). Size distributions of an emulsion stabilized with KryPEG(550) fluorosurfactants immediately after generation (red squares), after 26 days (blue circles) and after 90 days (green triangles).

short-term studies, emulsified by diblock and triblock fluorosurfactants composed of Krytox(FSH) and Jeffamine. Additionally, they investigate the short-term stability of emulsions after undergoing centrifugation, testing the fluorosurfactant's ability to stabilize emulsions under demanding conditions. Testing nanoemulsion stability using a mixture of elevated temperature, salts and potentially moderate agitation may demonstrate the use of our custom synthesized fluorosurfactants to be used as artificial oxygen carriers. In this application, long-term storage is imperative - making KryPEG(550) a suitable candidate for further testing. The monodisperse emul-

sion (from Figure 4.8) stabilized with KryPEG(550) has maintained a constant average droplet size for over one year, stored at room temperature (data not shown). Furthermore, over a span of 90 days, the size distribution of the emulsion stabilized with KryPEG(550) shows no significant broadening and maintains a consistent mean, median and mode over this time (Figure 5.2).

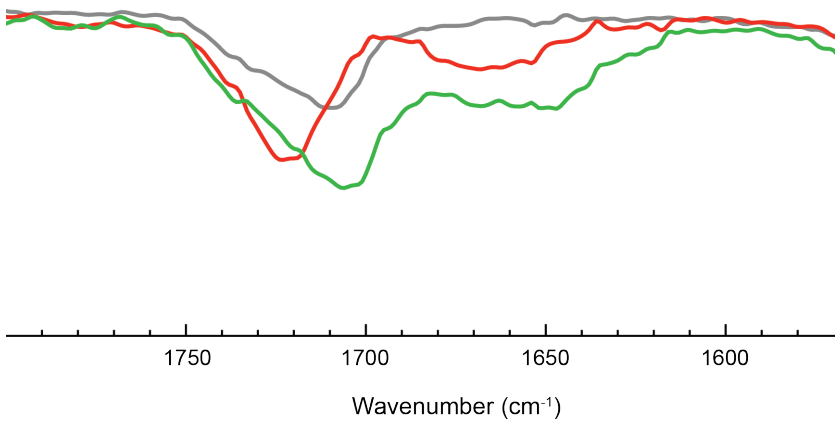

Figure 5.3: IR characterization of biotinylated fluorosurfactants. Region of interest cropped from the IR spectra of Krytox-NH_2 (gray), Kry-PEG(550) (red), and Kry-PEG(550)-biotin (green). While the Kry-PEG(550) fluorosurfactant shows an absorption band (at $\sim$1720 cm^{-1}) shifted from the Krytox-NH_2, the Kry-PEG(550)-biotin product does not.

Another extension of this work should aim to adapt functionalized fluorosurfactants to be utilized with droplets used as force transducers. In this case, functionalization of custom fluorosurfactants with biotin groups should be sought, which would replace the DSPE-PEG(2000)-biotin surfactant currently used. We conducted preliminary synthesis to achieve biotinylation of the fluorosurfactants, by replacing

the PEG head group with a biotinylated PEG molecule. The protocols established to synthesize the Kry-PEG(550) fluorosurfactant were followed in order to synthesize Kry-PEG(550)-biotin, however, this did not yield a successful product (Figure 5.3). We observed that the absorption band of Kry-PEG(550)-biotin coincided with that of the Krytox-NH_2 (both occurring at $\sim$1720 cm^{-1}), indicating that the reaction between Krytox-NH_2 and the amine-PEG-biotin was unsuccessful. This could be due to several reasons, including issues with solubility, since the biotin is hydrophobic, and its addition increases the molecular weight. The amine-PEG-biotin polymer was actually not soluble in the trifluorotoluene solvent typically used during the reaction used to synthesize Kry-PEG(550). Changing the reaction solvent to a mixture of chloroform and hexafluorobenzene also did not work. If this reaction were to be performed successfully, the biotinylated fluorosurfactants could be combined with the fluorosurfactants synthesized in Chapter 4 to achieve excellent long-term FC oil-in-water emulsion stability and enable facile preparation of functionlized, fluorescent droplets. This combination of surfactants could potentially improve the current system of droplets used as force transducers (introduced in Chapter 2), as the current system utilizes a non-fluorinated phospholipid surfactant which has been suspected to be limiting the current experimental lifetime of the droplets.

Bibliography

[1] Darcy Wentworth Thompson et al. On growth and form. *On growth and form.*, 1942.

[2] Malcolm S Steinberg. The problem of adhesive selectivity in cellular interactions. *Cellular membranes in development*, 1, 1964.

[3] Malcolm S Steinberg. Does differential adhesion govern self-assembly processes in histogenesis? equilibrium configurations and the emergence of a hierarchy among populations of embryonic cells. *Journal of Experimental Zoology Part A: Ecological Genetics and Physiology*, 173(4):395–433, 1970.

[4] Ramsey A Foty, Cathie M Pfleger, Gabor Forgacs, and Malcolm S Steinberg. Surface tensions of embryonic tissues predict their mutual envelopment behavior. *Development*, 122(5):1611–1620, 1996.

[5] Adam J Engler, Shamik Sen, H Lee Sweeney, and Dennis E Discher. Matrix elasticity directs stem cell lineage specification. *Cell*, 126(4):677–689, 2006.

[6] Fabien Montel, Morgan Delarue, Jens Elgeti, Danijela Vignjevic, Giovanni Cappello, and Jacques Prost. Isotropic stress reduces cell proliferation in tumor spheroids. *New Journal of Physics*, 14(5):055008, 2012.

[7] Annaïck Desmaison, Céline Frongia, Katia Grenier, Bernard Ducommun, and Valérie Lobjois. Mechanical stress impairs mitosis progression in multi-cellular tumor spheroids. *PloS one*, 8(12):e80447, 2013.

[8] Celeste M Nelson, Ronald P Jean, John L Tan, Wendy F Liu, Nathan J Sniadecki, Alexander A Spector, and Christopher S Chen. Emergent patterns of growth controlled by multicellular form and mechanics. *Proceedings of the National Academy of Sciences of the United States of America*, 102(33):11594–11599, 2005.

[9] Gang Cheng, Janet Tse, Rakesh K Jain, and Lance L Munn. Micro-environmental mechanical stress controls tumor spheroid size and morphology by suppressing proliferation and inducing apoptosis in cancer cells. *PLoS one*, 4(2):e4632, 2009.

[10] Sebastian J Streichan, Christian R Hoerner, Tatjana Schneidt, Daniela Holzer, and Lars Hufnagel. Spatial constraints control cell proliferation in tissues. *Proceedings of the National Academy of Sciences*, 111(15):5586–5591, 2014.

[11] Evan A Evans and David A Calderwood. Forces and bond dynamics in cell adhesion. *Science*, 316(5828):1148–1153, 2007.

[12] Jubin Kashef and Clemens M Franz. Quantitative methods for analyzing cell–cell adhesion in development. *Developmental biology*, 401(1):165–174, 2015.

[13] Dong Li, Jiaxi Zhou, Farhan Chowdhury, Jianjun Cheng, Ning Wang, and Fei Wang. Role of mechanical factors in fate decisions of stem cells. *Regenerative medicine*, 6(2):229–240, 2011.

[14] Xavier Trepat, Michael R Wasserman, Thomas E Angelini, Emil Millet, David A Weitz, James P Butler, and Jeffrey J Fredberg. Physical forces during collective cell migration. *Nature physics*, 5(6):426, 2009.

[15] Dhananjay T Tambe, C Corey Hardin, Thomas E Angelini, Kavitha Rajendran, Chan Young Park, Xavier Serra-Picamal, Enhua H Zhou, Muhammad H Zaman, James P Butler, David A Weitz, et al. Collective cell guidance by cooperative intercellular forces. *Nature materials*, 10(6):469, 2011.

[16] Olivia Du Roure, Alexandre Saez, Axel Buguin, Robert H Austin, Philippe Chavrier, Pascal Siberzan, and Benoit Ladoux. Force mapping in epithelial cell migration. *Proceedings of the National Academy of Sciences of the United States of America*, 102(7):2390–2395, 2005.

[17] Mina J Bissell and William C Hines. Why don't we get more cancer? a proposed role of the microenvironment in restraining cancer progression. *Nature medicine*, 17(3):320–329, 2011.

[18] Thomas Risler. Focus on the physics of cancer. *New Journal of Physics*, 17(5):055011, 2015.

[19] Sanjay Kumar and Valerie M Weaver. Mechanics, malignancy, and metastasis: the force journey of a tumor cell. *Cancer and Metastasis Reviews*, 28(1-2):113–127, 2009.

[20] Matthew J Paszek, Nastaran Zahir, Kandice R Johnson, Johnathon N Lakins, Gabriela I Rozenberg, Amit Gefen, Cynthia A Reinhart-King, Susan S Margulies, Micah Dembo, David Boettiger, et al. Tensional homeostasis and the malignant phenotype. *Cancer cell*, 8(3):241–254, 2005.

[21] Rakesh K Jain. An indirect way to tame cancer. *Scientific American*, 310(2):46, 2014.

[22] Douglas Hanahan and Robert A Weinberg. The hallmarks of cancer. *cell*, 100(1):57–70, 2000.

[23] Denis Wirtz, Konstantinos Konstantopoulos, and Peter C Searson. The physics of cancer: the role of physical interactions and mechanical forces in metastasis. *Nature reviews. Cancer*, 11(7):512, 2011.

[24] Jeroen Eyckmans and Christopher S Chen. 3d culture models of tissues under tension. *J Cell Sci*, 130(1):63–70, 2017.

[25] Brendon M Baker and Christopher S Chen. Deconstructing the third dimension–how 3d culture microenvironments alter cellular cues. *J Cell Sci*, 125(13):3015–3024, 2012.

[26] Rasheena Edmondson, Jessica Jenkins Broglie, Audrey F Adcock, and Liju Yang. Three-dimensional cell culture systems and their applications in drug discovery and cell-based biosensors. *Assay and drug development technologies*, 12(4):207–218, 2014.

[27] Otger Campas. A toolbox to explore the mechanics of living embryonic tissues. In *Seminars in cell & developmental biology*, volume 55, pages 119–130. Elsevier, 2016.

[28] William J Polacheck and Christopher S Chen. Measuring cell-generated forces: a guide to the available tools. *Nature methods*, 13(5):415, 2016.

[29] Kaoru Sugimura, Pierre-François Lenne, and François Graner. Measuring forces and stresses in situ in living tissues. *Development*, 143(2):186–196, 2016.

[30] Karine Guevorkian, Marie-Josée Colbert, Mélanie Durth, Sylvie Dufour, and Françoise Brochard-Wyart. Aspiration of biological viscoelastic drops. *Physical review letters*, 104(21):218101, 2010.

[31] JMt Mitchison and MM Swann. The mechanical properties of the cell surface. *Journal of Experimental Biology*, 31(3):461–472, 1954.

[32] Lap Man Lee and Allen P Liu. The application of micropipette aspiration in molecular mechanics of single cells. *Journal of nanotechnology in engineering and medicine*, 5(4):040902, 2014.

[33] Gabor Forgacs, Ramsey A Foty, Yinon Shafrir, and Malcolm S Steinberg. Viscoelastic properties of living embryonic tissues: a quantitative study. *Biophysical journal*, 74(5):2227–2234, 1998.

[34] Philippe Marmottant, Abbas Mgharbel, Jos Käfer, Benjamin Audren, Jean-Paul Rieu, Jean-Claude Vial, Boudewijn Van Der Sanden, Athanasius FM Marée, François Graner, and Hélène Delanoë-Ayari. The role of fluctuations and stress on the effective viscosity of cell aggregates. *Proceedings of the National Academy of Sciences*, 106(41):17271–17275, 2009.

[35] Keir C Neuman and Attila Nagy. Single-molecule force spectroscopy: optical tweezers, magnetic tweezers and atomic force microscopy. *Nature methods*, 5(6):491–505, 2008.

[36] Helene OB Gautier, Amelia J Thompson, Sarra Achouri, David E Koser, Kathrin Holtzmann, Emad Moeendarbary, and Kristian Franze. Atomic force

microscopy-based force measurements on animal cells and tissues. *Methods in cell biology*, 125:211–235, 2015.

[37] Kristian Franze. Atomic force microscopy and its contribution to understanding the development of the nervous system. *Current opinion in genetics & development*, 21(5):530–537, 2011.

[38] Wesley R Legant, Jordan S Miller, Brandon L Blakely, Daniel M Cohen, Guy M Genin, and Christopher S Chen. Measurement of mechanical tractions exerted by cells in three-dimensional matrices. *Nature methods*, 7(12):969–971, 2010.

[39] Karel Svoboda and Steven M Block. Biological applications of optical forces. *Annual review of biophysics and biomolecular structure*, 23(1):247–285, 1994.

[40] Hu Zhang and Kuo-Kang Liu. Optical tweezers for single cells. *Journal of The Royal Society Interface*, 5(24):671–690, 2008.

[41] Charlie Gosse and Vincent Croquette. Magnetic tweezers: micromanipulation and force measurement at the molecular level. *Biophysical journal*, 82(6):3314–3329, 2002.

[42] Zhongbo Yu, David Dulin, Jelmer Cnossen, Mariana Köber, Maarten M van Oene, Orkide Ordu, Bojk A Berghuis, Toivo Hensgens, Jan Lipfert, and Nynke H

Dekker. A force calibration standard for magnetic tweezers. *Review of Scientific Instruments*, 85(12):123114, 2014.

[43] ME Dolega, Morgan Delarue, François Ingremeau, Jacques Prost, Antoine Delon, and Giovanni Cappello. Cell-like pressure sensors reveal increase of mechanical stress towards the core of multicellular spheroids under compression. *Nature Communications*, 8:14056, 2017.

[44] Otger Campàs, Tadanori Mammoto, Sean Hasso, Ralph A Sperling, Daniel O'connell, Ashley G Bischof, Richard Maas, David A Weitz, Lakshminarayanan Mahadevan, and Donald E Ingber. Quantifying cell-generated mechanical forces within living embryonic tissues. *Nature methods*, 11(2):183–189, 2014.

[45] Quentin Brosseau, Jérémy Vrignon, and Jean-Christophe Baret. Microfluidic dynamic interfacial tensiometry (μdit). *Soft Matter*, 10(17):3066–3076, 2014.

[46] Adam A Lucio, Donald E Ingber, and Otger Campas. Generation of biocompatible droplets for in vivo and in vitro measurement of cell-generated mechanical stresses. *Methods in cell biology*, 125:373–390, 2015.

[47] C Holtze, AC Rowat, JJ Agresti, JB Hutchison, FE Angile, CHJ Schmitz, Sarah Köster, H Duan, KJ Humphry, RA Scanga, et al. Biocompatible surfactants for water-in-fluorocarbon emulsions. *Lab on a Chip*, 8(10):1632–1639, 2008.

[48] Linas Mazutis and Andrew D Griffiths. Selective droplet coalescence using microfluidic systems. *Lab on a Chip*, 12(10):1800–1806, 2012.

[49] Gordon F Christopher and Shelly L Anna. Microfluidic methods for generating continuous droplet streams. *Journal of Physics D: Applied Physics*, 40(19):R319, 2007.

[50] Micronit Microfluidics. Microfluidic droplet generators. *White Paper*, pages 3–4, 2010.

[51] Dolomite Microfluidics. Droplet junction chip characterisation. *Application Note*, pages 6–8, 2014.

[52] Linas Mazutis, John Gilbert, W Lloyd Ung, David A Weitz, Andrew D Griffiths, and John A Heyman. Single-cell analysis and sorting using droplet-based microfluidics. *Nature protocols*, 8(5):870, 2013.

[53] Ruei-Zhen Lin and Hwan-You Chang. Recent advances in three-dimensional multicellular spheroid culture for biomedical research. *Biotechnology journal*, 3(9-10):1172–1184, 2008.

[54] Franziska Hirschhaeuser, Heike Menne, Claudia Dittfeld, Jonathan West, Wolfgang Mueller-Klieser, and Leoni A Kunz-Schughart. Multicellular tumor

spheroids: an underestimated tool is catching up again. *Journal of biotechnology*, 148(1):3–15, 2010.

[55] Madeleine J Oudin and Valerie M Weaver. Physical and chemical gradients in the tumor microenvironment regulate tumor cell invasion, migration, and metastasis. In *Cold Spring Harbor Symposia on Quantitative Biology*, volume 81, pages 189–205. Cold Spring Harbor Laboratory Press, 2016.

[56] Tom PJ Wyatt, Andrew R Harris, Maxine Lam, Qian Cheng, Julien Bellis, Andrea Dimitracopoulos, Alexandre J Kabla, Guillaume T Charras, and Buzz Baum. Emergence of homeostatic epithelial packing and stress dissipation through divisions oriented along the long cell axis. *Proceedings of the National Academy of Sciences*, 112(18):5726–5731, 2015.

[57] Carsten Grashoff, Brenton D Hoffman, Michael D Brenner, Ruobo Zhou, Maddy Parsons, Michael T Yang, Mark A McLean, Stephen G Sligar, Christopher S Chen, Taekjip Ha, et al. Measuring mechanical tension across vinculin reveals regulation of focal adhesion dynamics. *Nature*, 466(7303):263, 2010.

[58] John L Tan, Joe Tien, Dana M Pirone, Darren S Gray, Kiran Bhadriraju, and Christopher S Chen. Cells lying on a bed of microneedles: an approach to isolate mechanical force. *Proceedings of the National Academy of Sciences*, 100(4):1484–1489, 2003.

[59] Tadanori Mammoto, Akiko Mammoto, and Donald E Ingber. Mechanobiology and developmental control. *Annual review of cell and developmental biology*, 29:27–61, 2013.

[60] Callie Johnson Miller and Lance Davidson. The interplay between cell signaling and mechanics in developmental processes. *Nature Reviews. Genetics*, 14(10):733, 2013.

[61] Celeste M Nelson and Mina J Bissell. Of extracellular matrix, scaffolds, and signaling: tissue architecture regulates development, homeostasis, and cancer. *Annu. Rev. Cell Dev. Biol.*, 22:287–309, 2006.

[62] Tiina Roose, Paolo A Netti, Lance L Munn, Yves Boucher, and Rakesh K Jain. Solid stress generated by spheroid growth estimated using a linear poroelasticity modelâŸĘ. *Microvascular research*, 66(3):204–212, 2003.

[63] Morgan Delarue, Jean-François Joanny, Frank Jülicher, and Jacques Prost. Stress distributions and cell flows in a growing cell aggregate. *Interface focus*, 4(6):20140033, 2014.

[64] Triantafyllos Stylianopoulos, John D Martin, Vikash P Chauhan, Saloni R Jain, Benjamin Diop-Frimpong, Nabeel Bardeesy, Barbara L Smith, Cristina R Ferrone, Francis J Hornicek, Yves Boucher, et al. Causes, consequences, and reme-

dies for growth-induced solid stress in murine and human tumors. *Proceedings of the National Academy of Sciences*, 109(38):15101–15108, 2012.

[65] Kévin Alessandri, Bibhu Ranjan Sarangi, Vasily Valérïévitch Gurchenkov, Bidisha Sinha, Tobias Reinhold Kießling, Luc Fetler, Felix Rico, Simon Scheuring, Christophe Lamaze, Anthony Simon, et al. Cellular capsules as a tool for multicellular spheroid production and for investigating the mechanics of tumor progression in vitro. *Proceedings of the National Academy of Sciences*, 110(37):14843–14848, 2013.

[66] Gabriel Helmlinger, Paolo A Netti, Hera C Lichtenbeld, Robert J Melder, and Rakesh K Jain. Solid stress inhibits the growth of multicellular tumor spheroids. *Nature biotechnology*, 15(8):778–783, 1997.

[67] Adele Khavari, Magnus Nydén, David A Weitz, and Allen J Ehrlicher. Composite alginate gels for tunable cellular microenvironment mechanics. *Scientific reports*, 6:30854, 2016.

[68] Hiroshi Kurosawa. Methods for inducing embryoid body formation: in vitro differentiation system of embryonic stem cells. *Journal of bioscience and bioengineering*, 103(5):389–398, 2007.

[69] Wenjun Zhang, Shuqi Wang, Min Lin, Yulong Han, Guiping Zhao, Tian Jian Lu, and Feng Xu. Advances in experimental approaches for investigating cell aggregate mechanics. *Acta Mechanica Solida Sinica*, 25(5):473–482, 2012.

[70] ELIJAH SHELTON, FRIEDHELM SERWANE, and OTGER CAMPÀS. Geometrical characterization of fluorescently labelled surfaces from noisy 3d microscopy data. *Journal of Microscopy*, 2017.

[71] Elizabeth E Robinson, Kathleen M Zazzali, Siobhan A Corbett, and Ramsey A Foty. Alpha5beta1 integrin mediates strong tissue cohesion. *Journal of cell science*, 116(Pt 2):377–386, January 2003.

[72] Morgan Delarue, J.-F. Joanny, F. Julicher, and Jacques Prost. Stress distributions and cell flows in a growing cell aggregate. *Interface Focus*, 4(6):20140033–20140033, oct 2014.

[73] Mary J Dorie, Robert F Kallman, Diane F Rapacchietta, Donna Van Antwerp, and Yi Rong Huang. Migration and internalization of cells and polystyrene microspheres in tumor cell spheroids. *Experimental cell research*, 141(1):201–209, 1982.

[74] Mary J Dorie, Robert F Kallman, and Marcia A Coyne. Effect of cytochalasin b, nocodazole and irradiation on migration and internalization of cells and mi-

crospheres in tumor cell spheroids. *Experimental cell research*, 166(2):370–378, 1986.

[75] Jean G Riess and Marie Pierre Krafft. Fluorinated materials for in vivo oxygen transport (blood substitutes), diagnosis and drug delivery. *Biomaterials*, 19(16):1529–1539, 1998.

[76] Vérpnique M Sadtler, Marie Pierre Krafft, and Jean G Riess. Achieving stable, reverse water-in-fluorocarbon emulsions. *Angewandte Chemie International Edition*, 35(17):1976–1978, 1996.

[77] Jean G Riess. Introducing a new element-fluorine-into the liposomal membrane. *Journal of Liposome Research*, 5(3):413–430, 1995.

[78] JG Riess. Fluorinated vesicles. *Journal of drug targeting*, 2(5):455–468, 1994.

[79] Marie Pierre Krafft. Fluorocarbons and fluorinated amphiphiles in drug delivery and biomedical research. *Advanced drug delivery reviews*, 47(2):209–228, 2001.

[80] Ernest G Schutt, Timothy J Pelura, and Ronald M Hopkins. Osmotically stabilized microbubble sonographic contrast agents. *Academic radiology*, 3:S188–S190, 1996.

[81] James C Knight, Peter G Edwards, and Stephen J Paisey. Fluorinated contrast agents for magnetic resonance imaging; a review of recent developments. *Rsc Advances*, 1(8):1415–1425, 2011.

[82] Matthew S Fox, Jeffrey M Gaudet, and Paula J Foster. Fluorine-19 mri contrast agents for cell tracking and lung imaging. *Magnetic resonance insights*, 8(Suppl 1):53, 2015.

[83] Jean G Riess. Oxygen carriers (âĂIJblood substitutesâĂİ) raison d'etre, chemistry, and some physiology blut ist ein ganz besondrer saft 1. *Chemical Reviews*, 101(9):2797–2920, 2001.

[84] Bernadette Remy, G Deby-Dupont, and Maurice Lamy. Red blood cell substitutes: fluorocarbon emulsions and haemoglobin solutions. *British medical bulletin*, 55(1):277–298, 1999.

[85] Jean G Riess. Blood substitutes: fluorocarbon approach. *Encyclopedia of Pharmaceutical Technology, 3rd Edition. New York: Informa Healthcare*, 336, 2007.

[86] Leland C Clark and Frank Gollan. Survival of mammals breathing organic liquids equilibrated with oxygen at atmospheric pressure. *Science*, 152(3730):1755–1756, 1966.

[87] Frank Gollan and LC Clark. Organ perfusion with fluorocarbon fluid. *Physiologist*, 9(191):H292, 1966.

[88] Jean G Riess. Reassessment of criteria for the selection of perfluorochemicals for second-generation blood substitutes: Analysis of structure/property relationships. *Artificial organs*, 8(1):44–56, 1984.

[89] R Naito and K Yokoyama. Perfluorochemical blood substitutes. *Technical information series*, (5), 1978.

[90] Alexey Kabalnov, Jeffry Weers, Rebecca Arlauskas, and Thomas Tarara. Phospholipids as emulsion stabilizers. 1. interfacial tensions. *Langmuir*, 11(8):2966–2974, 1995.

[91] Marcin Broniatowski and Patrycja Dynarowicz-Łątka. Semifluorinated alkanesâĂŤprimitive surfactants of fascinating properties. *Advances in colloid and interface science*, 138(2):63–83, 2008.

[92] Sabina Marie Bertilla, Jean-Louis Thomas, Pascal Marie, and Marie Pierre Krafft. Cosurfactant effect of a semifluorinated alkane at a fluorocarbon/water interface: impact on the stabilization of fluorocarbon-in-water emulsions. *Langmuir*, 20(10):3920–3924, 2004.

[93] Gianluca Etienne, Michael Kessler, and Esther Amstad. Influence of fluorinated surfactant composition on the stability of emulsion drops. *Macromolecular Chemistry and Physics*, 218(2), 2017.

[94] Daniel J Holt, Richard J Payne, and Chris Abell. Synthesis of novel fluorous surfactants for microdroplet stabilisation in fluorous oil streams. *Journal of Fluorine Chemistry*, 131(3):398–407, 2010.

[95] Milton J Rosen and Joy T Kunjappu. *Surfactants and interfacial phenomena*. John Wiley & Sons, 2012.

[96] Adam A Lucio, Alessandro Mongera, Elijah Shelton, Renwei Chen, Adele M Doyle, and Otger Campàs. Spatiotemporal variation of endogenous cell-generated stresses within 3d multicellular spheroids. *Scientific Reports*, 7(1):12022, 2017.

[97] Tharwat F Tadros. *Emulsion science and technology: a general introduction*. Wiley-VCH Verlag GmbH & Co. KGaA, 2009.

[98] Marie Pierre Krafft and Jean G Riess. Chemistry, physical chemistry, and uses of molecular fluorocarbon- hydrocarbon diblocks, triblocks, and related compounds- unique âĂIJapolarâĂİ components for self-assembled colloid and interface engineering. *Chemical reviews*, 109(5):1714–1792, 2009.

[99] Anika Nagelkerke, Johan Bussink, Fred CGJ Sweep, and Paul N Span. Generation of multicellular tumor spheroids of breast cancer cells: How to go three-dimensional. *Analytical biochemistry*, 437(1):17–19, 2013.

[100] Xue Gong, Chao Lin, Jian Cheng, Jiansheng Su, Hang Zhao, Tianlin Liu, Xuejun Wen, and Peng Zhao. Generation of multicellular tumor spheroids with microwell-based agarose scaffolds for drug testing. *PLoS One*, 10(6):e0130348, 2015.

[101] Juergen Friedrich, Claudia Seidel, Reinhard Ebner, and Leoni A Kunz-Schughart. Spheroid-based drug screen: considerations and practical approach. *Nature protocols*, 4(3):309–324, 2009.

[102] Amy L Howes, Robyn D Richardson, Darren Finlay, and Kristiina Vuori. 3-dimensional culture systems for anti-cancer compound profiling and high-throughput screening reveal increases in egfr inhibitor-mediated cytotoxicity compared to monolayer culture systems. *PloS one*, 9(9):e108283, 2014.

[103] Mariaceleste Aragona, Tito Panciera, Andrea Manfrin, Stefano Giulitti, Federica Michielin, Nicola Elvassore, Sirio Dupont, and Stefano Piccolo. A mechanical checkpoint controls multicellular growth through yap/taz regulation by actin-processing factors. *Cell*, 154(5):1047–1059, 2013.

[104] Matthew J Paszek and Valerie M Weaver. The tension mounts: mechanics meets morphogenesis and malignancy. *Journal of mammary gland biology and neoplasia*, 9(4):325–342, 2004.